Tectono-sedimentary evolution and petroleum systems of the Mundaú subbasin: A new deep-water exploration frontier in equatorial Brazil

Narelle Maia de Almeida, Tiago M. Alves, Francisco Nepomuceno Filho, George Satander Sá Freire, Ana Clara Braga de Souza, Márcio Nunes Normando, Karen M. Leopoldino Oliveira, and Thiago Henrique da Silva Barbosa

ABSTRACT

The Brazilian equatorial margin (BEM) evolved in response to transform motion between Brazil and Africa. In 2012, Petrobras drilled the Pecém well in the Mundaú subbasin (Ceará Basin) of the BEM to record the first deep-water oil discovery in the region. This work investigates the deep-water evolution of the Mundaú subbasin focusing on its structural and sedimentary evolution, and characterizes the petroleum systems in this new exploration frontier. For such purposes, poststack seismic reflection, borehole, and geochemical data were used. Three tectono-stratigraphic sequences representing synrift (Mundaú Formation), transitional (Paracuru Formation), and drift strata (Ubarana Formation) were divided into seven seismic units. Different tectonic domains were interpreted: proximal, distal, and Romanche Fracture Zone. Typical structures of transform margins, such as marginal ridges and marginal plateaus, were not identified in the Mundaú subbasin. Instead, the subbasin was predominantly deformed by transtensional movements. The Mundaú and Paracuru Formations are mature within the oil window, whereas the Ubarana Formation is immature. Main reservoir intervals consist of approximately 1-m (~3.28-ft)-thick intercalations of sandstone between shales, siltstones, and marls. The seal rocks comprise shales in the Ubarana Formation, whereas the hydrocarbon trap is related to an unconformity and a normal fault. This work concludes

AUTHORS

NARELLE MAIA DE ALMEIDA ~ *Programa de Pós-Graduação em Geologia, Universidade Federal do Ceará (UFC), Fortaleza, Ceará, Brazil; Instituto Federal do Rio Grande do Norte, Natal, Rio Grande do Norte, Brazil; narellemaia@gmail.com*

Narelle Maia de Almeida completed a B.Sc. in geology from UFC (2011), a master's degree in geodynamics and geophysics from the Federal University of Rio Grande do Norte (2014), and a Ph.D. in geology from UFC (2018). She is a professor at the Federal Institute of Rio Grande do Norte, Natal, and studies shallow and deep water on continental margins, sedimentary basins, marine and petroleum geology, and geophysics.

TIAGO M. ALVES ~ *3D Seismic Lab, School of Earth and Ocean Sciences, Cardiff University, Cardiff, United Kingdom; alvest@cardiff.ac.uk*

Tiago Alves completed a B.Sc. (1997) in engineering geology in Lisbon and a Ph.D. (2002) from the University of Manchester. He heads the 3D Seismic Lab, Cardiff University, since 2012. A sea-going marine researcher with close ties to the International Ocean Drilling Program, he undertakes research on deep-water continental margins, fluid migration in sedimentary basins, reservoir engineering, and geoenergy as an all-encompassing theme.

FRANCISCO NEPOMUCENO FILHO ~ *Departamento de Física, UFC, Fortaleza, Ceará, Brazil; nepomuceno@fisica.ufc.br*

Francisco Nepomuceno Filho holds a master's degree from University of Texas and a Ph.D. from the Universidade Estadual de Campinas. He worked at Petrobras as an executive manager for petroleum exploration and production in Brazil and as head of Petrobras's London office dedicated to presalt technology. He is coordinator of the Center of Excellence in Petroleum Geophysics and chief executive officer of the Technological Park of the UFC.

GEORGE SATANDER SÁ FREIRE ~ *Programa de Pós-Graduação em Geologia, UFC, Fortaleza, Ceará, Brazil; freire@ufc.br*

George Satander Sá Freire holds a B.Sc. in geology from the University of Fortaleza (1977), a master's degree in geosciences from the Federal University of Pernambuco (1985), and a Ph.D. in geology from Université de Nantes (1989). He is a professor at the UFC and has experience in geosciences, with emphasis on marine geology.

ANA CLARA BRAGA DE SOUZA ~ Programa de Pós-Graduação em Geologia, UFC, Fortaleza, Ceará, Brazil; anaclarageologia@alu.ufc.br

Ana Clara B. Souza is a Ph.D. student at UFC. She currently works in the Center of Excellence in Petroleum Geophysics. Her research involves sequence stratigraphy and the characterization of hydrocarbon reservoirs on the equatorial margin of Brazil. Previous experience includes facies analysis and the characterization of unconventional petroleum system in Paleozoic basins of northeastern Brazil.

MÁRCIO NUNES NORMANDO ~ Programa de Pós-Graduação em Geologia, UFC, Fortaleza, Ceará, Brazil; mnormando@gmail.com

Márcio N. Normando is a senior reservoir modeler and Ph.D. student in the geology department at UFC. His research area comprises the geostatistical and geological modeling of reservoirs in the Ceará Basin. He worked for 11 years at Beicip-Franlab in integrated reservoir studies before starting his Ph.D. in 2016.

KAREN M. LEOPOLDINO OLIVEIRA ~ Programa de Pós-Graduação em Geologia, UFC, Fortaleza, Ceará, Brazil; karenleopoldino@gmail.com

Karen M. L. Oliveira is an M.Sc. geologist and Ph.D. student at UFC, developing a project between the Center of Excellence in Petroleum Geophysics and the Geophysics Laboratory at UFC, focusing on the Brazilian equatorial margin. Her research areas are geophysics applied to study of sedimentary basins and petroleum geophysics. She has experience as an instructor and researcher in projects using applied geophysics.

that the Paracuru Formation is the main source and reservoir in the deep-water Mundaú subbasin, effectively comprising a Paracuru–Paracuru petroleum system. The results have significant implications for petroleum exploration in the BEM by proposing a developed transitional petroleum system in the distal parts of northeastern Brazil.

INTRODUCTION

Transform margins are formed by rifting continental crust that is increasingly thinned as adjacent continents progressively move apart. Eventually, newly formed oceanic crust is juxtaposed against the continental margin on the opposite oceanward side of the transform fault (Mascle and Blarez, 1987). Despite the multitude of studies about transform margins published in the last 45 yr, focused on regions such as offshore Agulhas, Africa (Dingle, 1973; Scrutton, 1973, 1976; Ben-Avraham et al., 1997), Côte d'Ivoire-Ghana (Arens et al., 1971; Delteil et al., 1974; Mascle and Blarez, 1987; de Caprona, 1992; Basile et al., 1993), Brazil equatorial margin (BEM) (Zalán, 1985; Zalán et al., 1985; Nemčok et al., 2012; Krueger et al., 2014; Davison et al., 2016), Exmouth Plateau, Australia (Lorenzo et al., 1991), Gulf of California (Bischoff and Henyey, 1974; Moore and Curray, 1982; Lonsdale, 1985), and Newfoundland, North Atlantic (Todd et al., 1988; Keen et al., 1990), as well as synthesis studies and reviews (Scrutton, 1976, 1979, 1982; Lorenzo and Wessel, 1997; Reid and Jackson, 1997; Bird, 2001; Basile, 2015; Mercier de Lépinay et al., 2016), this type of margin is poorly understood when compared to its divergent and convergent counterparts. Transform margins are also difficult to investigate because of their relative steepness and complex geometries, in particular near intersections with rifted divergent margins (Mercier de Lépinay et al., 2016). Furthermore, the economic interest in transform margins is relatively new as they became a significant target for industry only after the discovery of the Jubilee field, offshore Ghana, in 2007 (Dailly et al., 2013; Mercier de Lépinay et al., 2016).

Considerable progress has been made in terms of understanding how tectonic and sedimentary processes interact in shallow parts of the Ceará Basin, BEM (Zalán, 1985; Zalán et al., 1985; Costa et al., 1990; Beltrami et al., 1994; Morais Neto et al., 2003; Condé et al., 2007; Antunes et al., 2008) (Figure 1). However, detailed seismic stratigraphic, depositional, and structural frameworks for deep-water areas of the Ceará Basin are still lacking in the published literature. Published seismic interpretations in deep-water Ceará have never been fully validated because of the absence of well ties. In 2012, Petrobras (Petróleo Brasileiro, SA) drilled the Pecém well (1_BRSA_1080) responsible

for the first deep-water oil discovery in Ceará Basin (Figures 1, 2). This well provided, for the first time, stratigraphic ties for the deep-water Mundaú subbasin, which is the focus of this paper.

This paper aims to investigate the tectono-stratigraphic evolution of the deep-water Mundaú subbasin, the only hydrocarbon producing region offshore Ceará, focusing on the geometries and nature of faults, as well as on structural and sedimentary restorations. Novel interpretations of multichannel seismic reflection data, borehole, and geochemical data from the deep-water Mundaú subbasin, along the westernmost segment of the Romanche Transform Fault Zone (Figure 1), are presented. This study addresses the following research questions.

1. What are the major variations, magnitude(s) and timing(s) of deposition in deep-water Mundaú?
2. What is the structural framework of this margin in its deep-water region?
3. In what way does the deep-water tectono-stratigraphic evolution contribute to a complete knowledge of petroleum systems along the BEM?

GEOLOGICAL SETTING

Equatorial Atlantic Ocean Opening

Continental breakup occurred first in the southern South Atlantic (southern branch) during the Early Cretaceous, progressing into the equatorial Atlantic (equatorial branch) by the Albian (Matos, 1992; Moulin et al., 2010). Nemčok et al. (2015) considered that the initial stress field controlling the development of a transform fault system in the equatorial Atlantic was able to develop a right-stepping system in east-northeast dextral strike-slip fault zones. Shear orientations indicate that the positions of fault zones were controlled by prominent crustal weaknesses in equatorial Brazil, namely northeast-striking features associated with Proterozoic and Paleozoic basement structures (Mascle et al., 1988; Genik, 1992; Guiraud and Maurin, 1992). In addition, Moulin et al. (2010) and other authors (e.g., Nürnberg and Müller, 1991; Macdonald et al., 2003; König and Jokat, 2006; Eagles, 2007) suggested significant intraplate deformation in both Africa and South America during Atlantic opening. On the South American plate, Moulin et al. (2010) inferred 10–20 km (6.2–12.4 mi) of extension in the northeastern Brazil block, along the Potiguar and Araripe Basins, 50–60 km (31.1–37.3 mi) of extension in the Tucano Basin, and 60 km (37.3 mi) of dextral strike-slip motion along the Transbrasiliano lineament (Figures 1, 2). Their paleogeographic

THIAGO HENRIQUE DA SILVA BARBOSA ~ *Departamento de Engenharia do Petróleo, UFC, Fortaleza, Ceará, Brazil* *thiagohenrique@alu.ufc.br*

Thiago H. S. Barbosa is a petroleum engineer and graduate student in the chemical engineering program of UFC. His research interests include reservoir modeling and characterization, phase behavior of reservoir fluids, and numerical reservoir simulation. His experience involves projects centered on marginal oil fields located in the Brazilian equatorial margin.
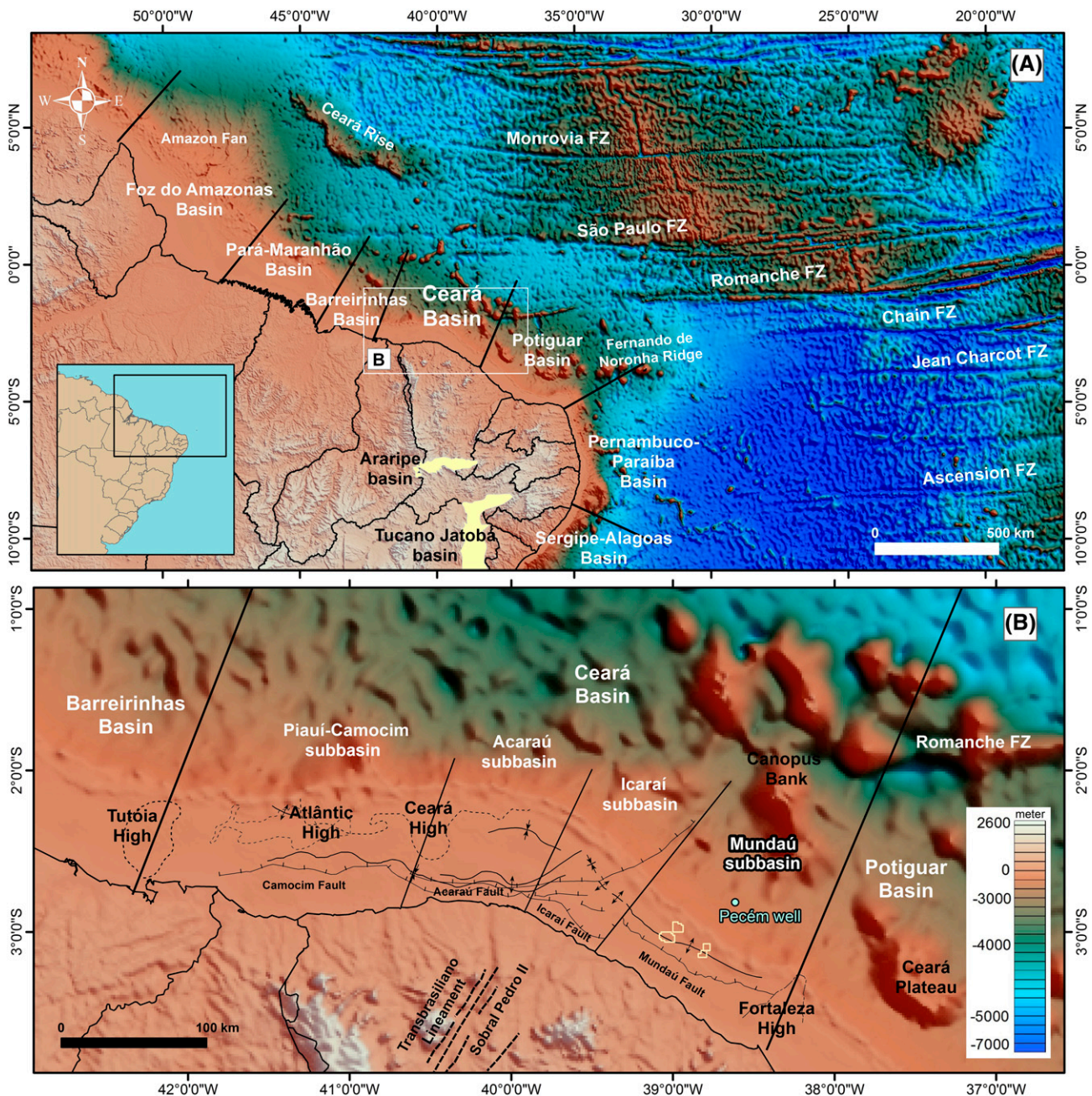
Figure 1. (A) Map of the northeast Brazilian margin depicting the location of sedimentary basins on the Brazilian equatorial margin (Foz do Amazonas, Pará-Maranhão, Barreirinhas, Ceará, and Potiguar basins), as well as the larger fracture zones in the area. (B) The Ceará Basin is compartmentalized into four subbasins: Piauí–Camocim, Acaraú, Icaraí, and Mundaú. The study area is located in the Mundaú subbasin. The topographic model was provided by the Brazilian Geological Service. The structural data were compiled from Zalán (1985), Silva et al. (1998), and Morais Neto et al. (2003). The basin boundaries were provided by Brazilian National Petroleum Agency and the subbasins boundaries were adapted from Morais Neto et al. (2003). FZ = fault zone.

model shows that opening of the equatorial Atlantic Ocean occurred during the Aptian–Albian and supports the hypothesis of a northward propagation of the South American deformation, as proposed by Eagles (2007).

The initial propagation of intracontinental strike-slip zones in the equatorial Atlantic started by progressively extending a transtensional setting (Szatmari, 2000). Dextral shear was responsible for crustal rupture, resulting in the generation of a
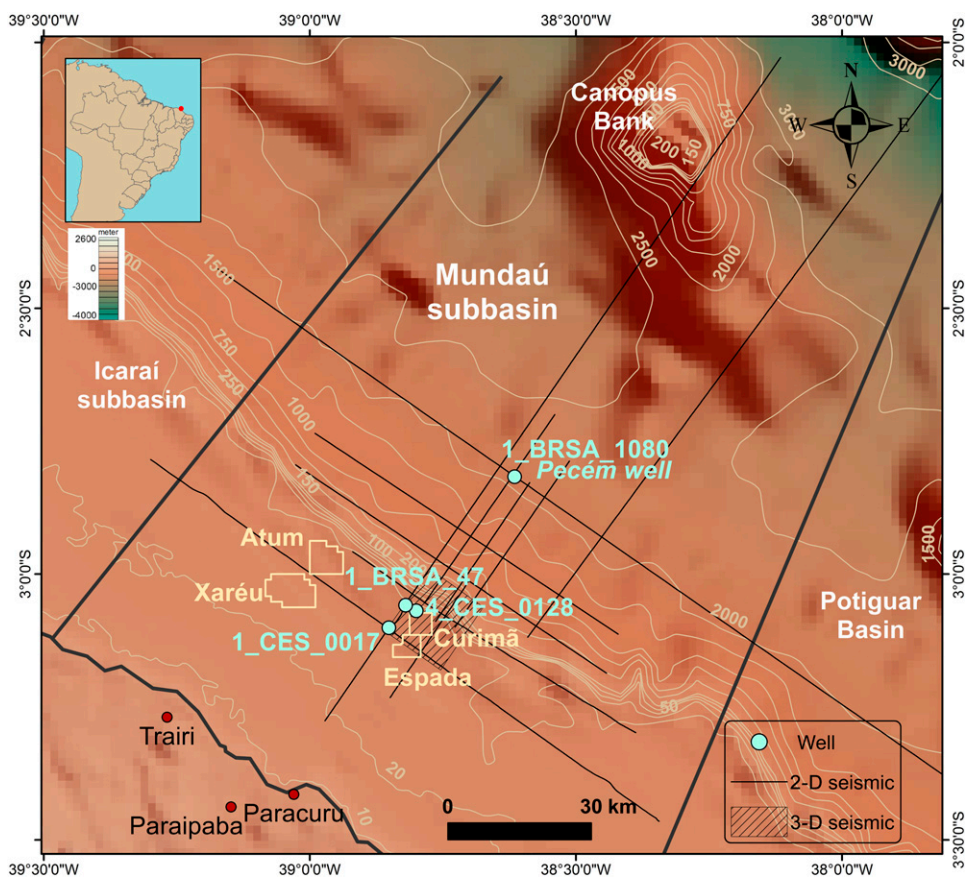
Figure 2. Four producing fields (Xaréu, Atum, Curimã, and Espada) in the Mundaú subbasin. The location of the wells and seismic data (two-dimensional [2-D] and three-dimensional [3-D]) are shown on the bathymetric map. The bathymetric data were provided by the Brazilian Geological Service.

complex pattern of subvertical oblique faults that controlled the rift geometry of the BEM, which later evolved into large oceanic fracture zones parallel to the coast (Gorini and Bryan, 1976). These fault zones include the Chain Fracture Zone (CFZ), Romanche Fracture Zone (RFZ), and São Paulo Fracture Zone (Figure 1).

According to Davison et al. (2016), the RFZ was originally an Aptian corridor of dextral transtensional rifting along the margins of the equatorial Atlantic. A transpressional tectonic episode occurred at the time to produce large folds, thrusts, and positive flower structures throughout the Barreirinhas and Ceará Basins of equatorial Brazil (Zalán, 1985), and also along the Ghana–Togo–Benin–West Nigeria segment of the African margin (Figure 1). The two fold belts were then separated by continued opening of the equatorial Atlantic Ocean (Davison et al., 2016).

Brazilian Equatorial Margin

The BEM comprises the Foz do Amazonas, Pará-Maranhão, Barreirinhas, Ceará, and Potiguar Basins (Figure 1). The BEM is characterized by the presence of east-west segments and northwest-southeast segments, forming en echelon features that are typically associated with strike-slip movement on transform margins (Gorini, 1993). This margin is also affected by gravitational tectonic processes (Silva et al., 1998; Cobbold et al., 2004; Reis et al., 2010, 2016; Oliveira et al., 2012). Silva et al. (1998) were the first authors to identify a linked extensional–compressional system gliding over two surfaces of weak overpressured shales, likely induced by progradation and overloading of the Amazon fan (Foz do Amazonas Basin): (1) a lower decollement placed at the top of the Lower Cretaceous marine megasequence (ca. 100 Ma), and (2) an intermediate decollement at the base of the Paleocene–Eocene marine megasequence (ca. 65 Ma).

MAIA DE ALMEIDA ET AL. **799**

Cobbold et al. (2004) attributed hydrocarbon generation as the best explanation for the presence of a decollement in Cretaceous rocks. The broadly triangular area of detachment coincides with an inferred pod of Cenomanian–Turonian source rock, which was interpreted to have been in the gas window during the decollement's formation. In the Pará–Maranhão and Barreirinhas Basins, the gravitational system is characterized by thrusts developed in a classical backstepping sequence, with younger thrusts developing on the hanging wall and showing marked landward migration of depocenters through time (Oliveira et al., 2012).

All the gravitational systems known on the BEM occur in drift sequences (Silva et al., 1998, 2010; Cobbold et al., 2004; Oliveira et al., 2012; Reis et al., 2016).

Ceará Basin and Mundaú Subbasin

The Ceará Basin is bounded to the east by the Fortaleza High, to the west by the Tutóia High, to the south by basement rocks, and to the north by the RFZ (Figure 1) (Costa et al., 1990). Because of the distinct tectonic character along and across the margin, the Ceará Basin has been divided into four subbasins, from east to west: Mundaú, Icaraí, Acaraú, and Piauí–Camocim (Figure 1). The Piauí–Camocim is separated from the Acaraú subbasin by the Ceará High (Figure 1B). The Acaraú and Icaraí subbasins have, as a common limit, the Sobral–Pedro II lineament. In addition, the Icaraí is separated from the Mundaú subbasin by an important fault inflection (Morais Neto et al., 2003) (Figure 1B).

The tectono-sedimentary evolution of the Mundaú subbasin consists of three major megasequences (Beltrami et al., 1994): synrift, transitional, and drift. The synrift phase is characterized by the development of northwest-southeast normal faults forming asymmetric half grabens, and continental sedimentation marked by fluvial–deltaic sandstones and shales of the Mundaú Formation, particularly toward proximal parts of the margin (Beltrami et al., 1994) (Figure 3).

The transitional sequence (upper Aptian to lower Albian) is marked by the first marine incursions recorded in the subbasin, comprising fluvial, deltaic, and lacustrine sandstones. Limestones and subordinate evaporites were also deposited at this stage. These rocks comprise the Paracuru Formation (Costa et al., 1990; Beltrami et al., 1994; Condé et al., 2007) (Figure 3).

The drift or marine megasequence (Albian to Holocene), developed in association with continental drift, records a phase of thermal subsidence on the whole of the BEM. The Ubarana Formation comprises two members (Figure 3). The first one, the Uruburetama Member, corresponds to a marine transgression spanning from the Albian to the Campanian, and predominantly consists of shales. The second member, Itapagé Member, correlates with a regressive marine phase developed from Campanian to Eocene, and comprises turbiditic shales and sandstones (Costa et al., 1990; Beltrami et al., 1994; Condé et al., 2007).

The Guamaré Formation consists of shelf carbonates, whereas the Tibau Formation comprises proximal sandstones. The clastic continental strata of the Barreiras Formation (Miocene–Holocene) comprises the youngest unit in the basin (Condé et al., 2007) (Figure 3).

Magmatism in the Ceará Basin occurred between the middle Eocene and early Oligocene. It was associated with a mafic event represented by intrusive bodies of basalt and diabase, some of which were sampled in several exploration wells (Condé et al., 2007). Data from K-Ar and Rb-Sr (Mizusaki et al., 2002) indicate that volcanic rocks range in age from the Eocene (44 Ma) on the Ceará High, to the Oligocene (32 Ma) on the Fortaleza High. Locally, near the Xaréu field (Figure 2), a diabase provided a K-Ar age at circa 83 Ma, and may be related to the Cuó magmatic event—also recorded in the Potiguar Basin and dated as Santonian–Turonian (Condé et al., 2007).

The Mundaú subbasin is an oil- and gas-producing basin with four fields in its shallow waters (Xaréu, Atum, Espada, and Curimã) (Figure 2). Exploration started in the 1970s and has continued until the present day. In 2012, Petrobras recorded the first deep-water discovery in the Pecém well. According to the Brazilian National Petroleum Agency (ANP), in situ volumes are estimated at 4.9 billion bbl of oil. The region is particularly attractive because it has already established infrastructure for hydrocarbon transport and downstream activities.
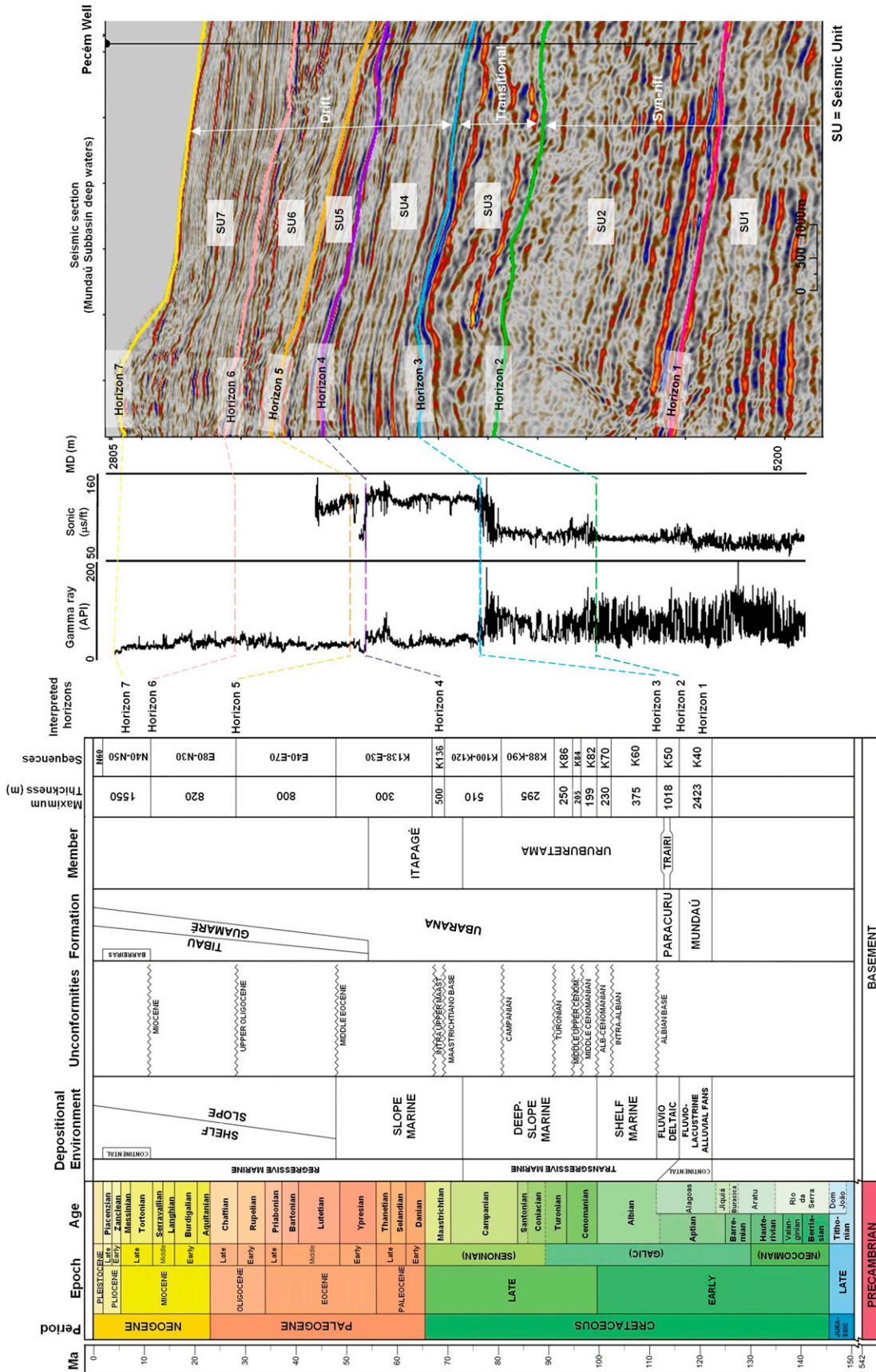
Figure 3. Correlation panel among interpreted seismic units (SU), stratigraphic information from the Ceará Basin (Condé et al., 2007), gamma-ray and sonic logs at the Pecém well. MD = measured depth.

DATA AND METHODS

For this study, (1) seismic, (2) well, (3) chronostratigraphic, and (4) geochemical data from the Pecém well were used. The data were obtained by Petrobras and supplied by ANP.

The seismic data comprise approximately 900 km (~560 mi) of poststack time-migrated multichannel two-dimensional seismic reflection profiles, with a sample interval of 4.0 ms, covering an area of approximately 12,800 km^2 (~4940 mi^2) (Figure 2). Two regional seismic lines reach 18,000 ms two-way traveltime (twt) depth, whereas others reach approximately 7000 ms twt.

A three-dimensional (3-D) seismic volume was used to correlate the shallow and deep-water data sets. The 3-D seismic volume consists of 172 inlines spaced 75 m (246.1 ft), and 663 crosslines spaced 25 m (82.0 ft). The inline length is 16.6 km (10.3 mi) and the crossline is 12.8 km (8.0 mi), comprising a total area of 212 km^2 (81.9 sq mi). The seismic volume images strata to a depth of 5000 ms twt.

Seismic–stratigraphic interpretations were undertaken based on data from exploration wells 1_BRSA_1080 (Pecém well), 1_BRSA_47, 1_CES_0017, and 4_CES_128, drilled by Petrobras (Figure 2). Well data include standard log suites (e.g., gamma-ray [GR], sonic [DT], density, and resistivity), check-shot surveys, lithologic data, formation tops, and biostratigraphic ages.

Seismic interpretation was performed using Schlumberger's Petrel®. Seismic analysis was conducted based on the general principles of seismic stratigraphy considering the seismic patterns such as seismic terminations, seismic facies, and seismic units (SU) (Mitchum et al., 1977; Catuneanu, 2006). Firstly, chronostratigraphic information was plotted on the seismic lines. Then, the most significant seismic reflectors were mapped in terms of continuity and amplitude to define discrete seismic sequences. The data set was interpreted in twt.

Geochemical information from the Pecém well includes total organic carbon (TOC) and Rock-Eval pyrolysis data. For the determination of organic carbon content (TOC), a small fraction of each sample was powdered, weighed, and chemically treated with hydrochloric acid to remove any inorganic carbon (carbonate). Samples were washed, dried, and analyzed using a LECO apparatus, which directly provided the weight percentage of TOC. The TOC content was evaluated according to Peters and Cassa (1994) classification (Table 1). For samples displaying a TOC content of approximately 1%, sediments were further submitted to Rock-Eval pyrolysis analyses. The pyrolysis analyses were performed with a Rock-Eval apparatus following the method described by Espitalié et al. (1977, 1985).

Espitalié et al. (1977) stated that the first peak (S_1) represents the amount of free hydrocarbon (milligrams of HC per gram of sediment), vaporized at 300°C. The second peak (S_2) is the amount of hydrocarbon released from cracking organic compounds (milligrams of HC per gram of sediment) and

Table 1. Classification of Total Organic Carbon Content, Potential Generator of Organic Matter and Hydrogen Index, Production Index, and Migration Index

Parameter	Classification
Total organic carbon*	
<0.5	Poor
0.5–1.0	Moderate
1.0–2.0	Good
2.0–4.0	Very good
>4.0	Excellent
Generation potential of organic matter[†]	
<2.0	Low source potential generator
2.0–5.0	Moderate source potential
5.0–10.0	Good source potential
>10.0	Excellent source potential
Hydrogen index[†]	
<200	Gas potential
200–300	Gas and condensate potential
>300	Oil potential
Production index[‡]	
<0.10	Immature
0.10–0.30	Mature (oil generation)
>0.30	Overmature (gas generation and destruction)
Migration index[§]	
<1.5	Autochthonous hydrocarbons
>1.5	Allochthonous hydrocarbons

*According to Peters and Cassa (1994).
[†]Based on Espitalié et al. (1977, 1985).
[‡]Based on Peters and Cassa (1994).
[§]Based on Peters (1986) and Hunt (1996).

heavy hydrocarbons during temperature programmed pyrolysis (300°C–600°C), being related to the residual hydrocarbon source potential. The S_3 peak represents the amount of CO_2 resulting from breaking carboxyl groups and other oxygen-containing compounds obtained at 300°C–390°C.

The hydrogen index (HI) ($HI = (S_2/TOC) \times 100$ in milligrams of HC per gram of TOC) and oxygen index (OI) ($OI = (S_3/TOC) \times 100$ in milligrams of CO_2 per gram TOC) were calculated following the procedures of Espitalié et al. (1977). The HI is a parameter used to characterize the origin of organic matter. Marine organisms and algae are, in general, composed of lipid- and protein-rich organic matter in which the H/C ratio is relatively higher than in the carbohydrate-rich constituents of land plants (Espitalié et al., 1977). Thus, HI typically ranges from approximately 100 to 600 in marine geological samples. The OI is a parameter that correlates with the O/C ratio, and it is related to the amount of oxygen in organic compounds. The OI is high for polysaccharide-rich remains of land plants and inert for organic material in marine sediments. The OI values range from near 0 to approximately 150 (Espitalié et al., 1977).

The production index (PI) ($PI = S_1/(S_1 + S_2)$) is the ratio of the amount of free hydrocarbons already generated compared with the total amount of hydrocarbon that rocks can generate (Peters and Cassa, 1994). The maximum temperature (T_{max}) is recorded at the maximum of hydrocarbon generation during pyrolysis, and it is used as a kerogen maturation rank evaluation (Espitalié et al., 1977, 1985). The migration index (S_1/TOC) was calculated based on Peters (1986). The range in values typical of source rocks is shown in Table 1.

RESULTS

Seismic Stratigraphy

Three principal tectono-stratigraphic sequences representing synrift, transitional, and drift strata were subdivided into seven SU (Figures 3–6).

Seismic Unit 1: Lower Cretaceous (Synrift I)

The lower boundary of SU1 is marked by a surface of moderate to high amplitude, locally diffusive, and is interpreted as comprising the top basement (Figures 4, 7, 8). The SU1 shows moderate- to high-amplitude seismic reflections in its upper part and low- to high-amplitude reflections in its lower part. All reflections dip oceanward. At the location of the Pecém well, seismic reflections become horizontal and subparallel (Figure 5).

On the continental shelf, SU1 is tilted by oceanward-dipping faults, whereas on the continental slope and abyssal plain it is cut by landward and oceanward-dipping, high-angle extensional and rollover faults (Figures 4, 5). The unit fills asymmetric half grabens showing a maximum thickness of approximately 2500 ms in shallow waters, and approximately 3750 ms in deep waters. It also presents growth faults (Figure 5). The SU1 comprises strata deposited in early synrift time.

The upper boundary of SU1 consists of the extension, from shallow to deep waters, of a continuous high-amplitude seismic reflection that coincides with the electric mark 80 (Costa et al., 1990) or 800 (Condé et al., 2007) (Figures 4, 5, 7, 8).

Seismic Unit 2: Lower Cretaceous to Lower Aptian (Synrift II)

Strata in the lower part of SU2 are of moderate to high amplitude and, in its upper part, of low amplitude and high frequency (Figures 3, 5). The SU2 becomes thicker toward deep-water areas and most of the imaged faults intersect it in its entirety. Similarly to SU1, SU2 fills asymmetric half grabens and presents growth faults (Figures 4, 5, 7).

The upper boundary of SU2 coincides with the high-amplitude Aptian electric mark 100 (Costa et al., 1990) or 1000 (Condé et al., 2007) recognized on the continental shelf (Figures 5, 7, 8). Both SU1 and SU2 correlate with the Mundaú Formation, which, based on the Pecém well, is composed of interbedded continental sandstone, siltstone, and shale (Figure 6).

Seismic Unit 3: Lower Aptian to Upper Aptian (Transitional Sequence)

The SU3 is composed of subparallel, locally transparent to high-amplitude seismic reflections. In Figure 5D, SU3 is observed at the crest of a rollover anticline. It presents growth onto major normal faults, highlighting active tectonic subsidence in
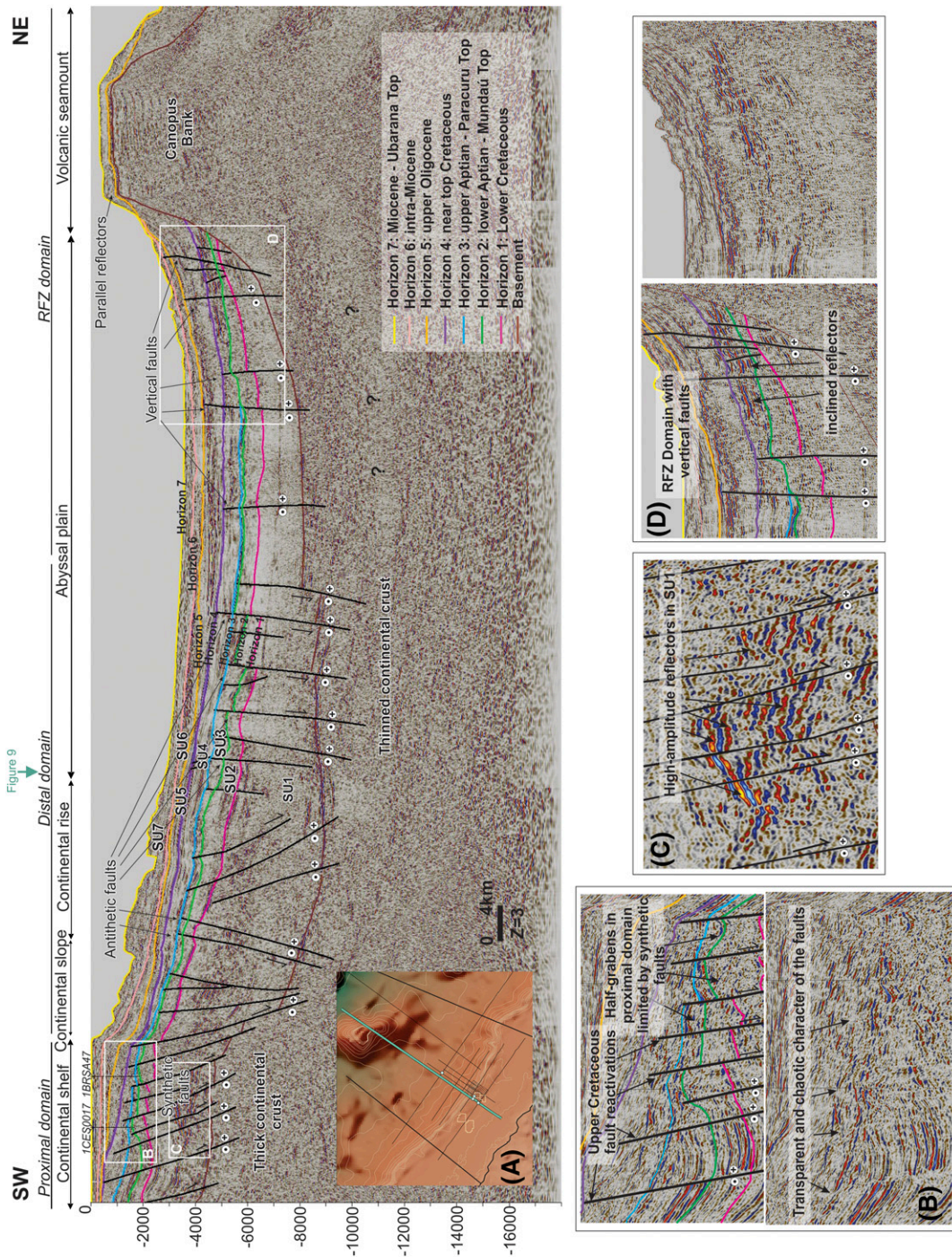
Figure 4. Seismic section showing the proximal, distal, and Romanche Fracture Zone (RFZ) domains in the study area. In the proximal domain (continental shelf), basinward-dipping extensional faults form multiple half grabens. The distal domain is characterized by high-angle landward and basinward-dipping faults. The distal domain includes the continental slope, continental rise, and abyssal plain. The RFZ domain is characterized by subvertical faults and a volcanic seamount. Thick continental crust is interpreted in the proximal domain, while thin continental crust is observed in the distal domain. A high-reflectivity zone approximately 8000 ms two-way traveltime (twt) is interpreted as marking the transition from sedimentary sequences to the continental crust. Vertical scale in twt. (A) Location of the seismic data. (B) Synrift faults were reactivated near the top of Cretaceous strata, forming multiple half grabens. The figure also shows the diffuse to chaotic character of the faults. (C) Very high-amplitude reflectors in SU1. (D) Vertical faults of the RFZ domain. Vertical exaggeration (Z) is 3 in (A) and 5 in (B)–(D). SU = seismic unit.

804   Evolution and Petroleum Systems of Deep-Water Mundaú Subbasin
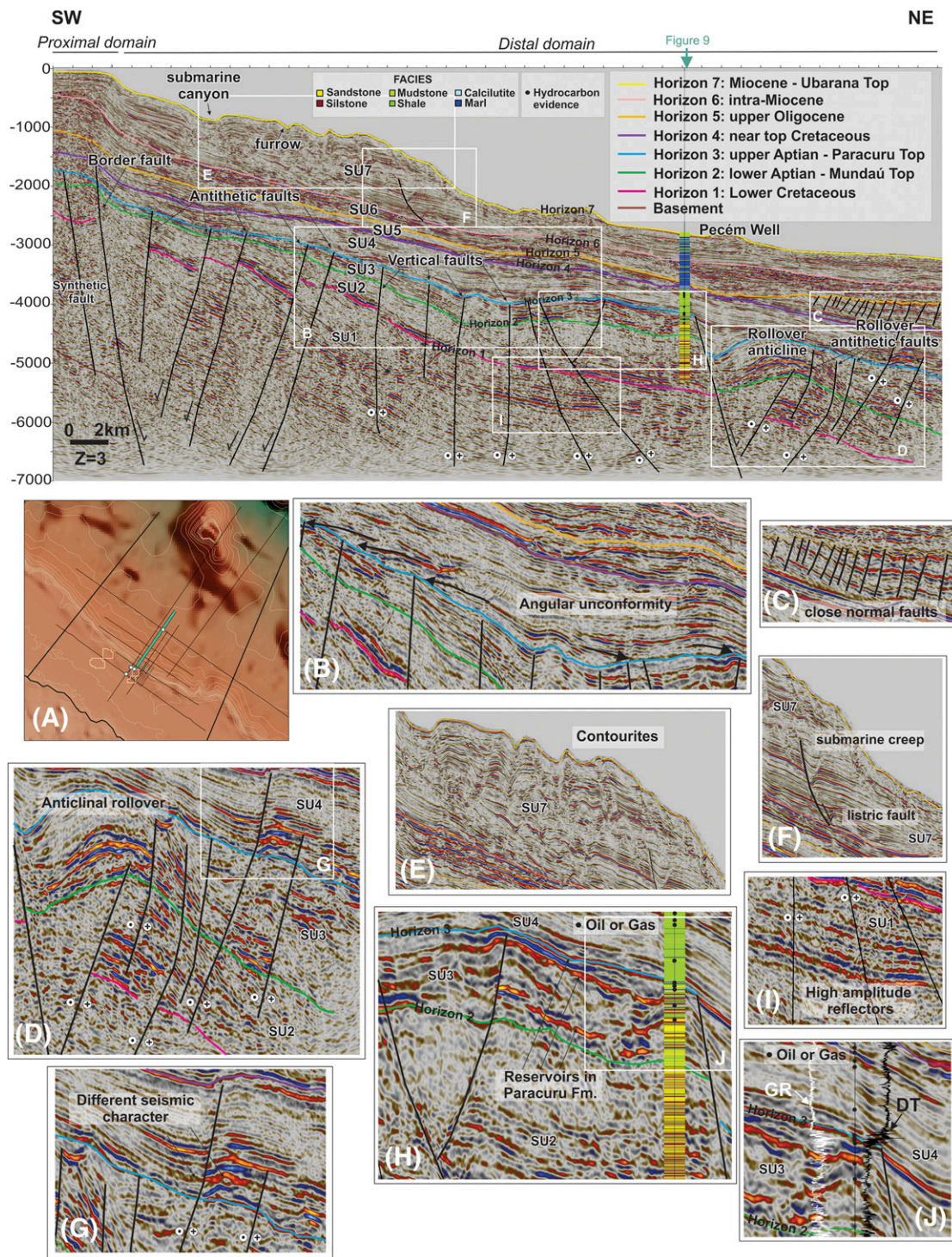
Figure 5. Southwest-northeast seismic section showing the proximal domain with synthetic faults and the distal domain with antithetic faults. The location of the Pecém well, the first oil discovery well in deep-water Ceará Basin, is shown together with facies and the location of hydrocarbon shows. Vertical scale in two-way traveltime (meters per second). (A) Location of the seismic data. (B) Horizon 3 comprises an angular unconformity between seismic unit 3 (SU3) and SU4. (C) Closely spaced normal faults in the distal domain. (D) Faulted rollover anticline. (E) Wavy and plastered reflectors typical of contourites in SU7. (F) Small-scale submarine creep in SU7. (G) Differing seismic characters across a normal fault. (H) Very thin sandstones reservoirs in the Paracuru Formation (Fm.) top (SU3) among shales, siltstones and marls. (I) High-amplitude seismic reflectors in SU1. (J) Abrupt changes in gamma-ray (GR) and sonic (DT) logs when crossing horizon 3. Vertical exaggeration (Z) is 3 in (A) and 5 in (B) to (J).

MAIA DE ALMEIDA ET AL. **805**

Seismic units	Lithology	Age of top	Top MD (m)	Thick-ness (m)	Top MD (ft)	Thick-ness (ft)	Tectonic Stage	Internal character, geometry and terminations	Lithology description	Importance in petroleum system
SU7		Miocene	2157	443	7077	1453	Drift	Chaotic to continuous as internal pattern, low- to medium-amplitude reflections, high frequency, interrupted by submarine canyons.	Marls, shales, clays, and calcilutites.	Overburden rocks
SU6		intra-Miocene	2600	386	8530	1267		Prograding high-amplitude reflections. Chaotic to continuous reflections.	Marls, shales, sandstones, and calcilutites.	Overburden rocks
SU5		late Oligocene	2986	90	9797	295		Locally transparent, very low-amplitude, subparallel, and prograding reflectors.	Greenish light gray marl, local pyrite, soft to semihard. Fine hyaline sandstone, subrounded, well sorted, disaggregated. White calcilutite, soft to semihard.	Overburden rocks
SU4		near top Cretaceous	3076	607	10092	1991		Continuous, parallel, low-amplitude, and medium- to high frequency, rather transparent. Onlap terminations.	Greenish, dark to light gray shale, carbonaceous, semihard. Hyaline sandstone, fine to very fine, subrounded to subangular, well to moderately sorted, disaggregated. Light gray marl, soft to semihard.	Seal
SU3		late Aptian	3683	647	12083	2123	Transitional	Subparallel, high-amplitude reflectors. Low frequency.	Greenish dark gray shales, slightly carbonaceous, semihard to hard. Brownish clay sandstone, very fine to coarse, angular to rounded, well sorted, porosity between 0 and 15%, compact to semi friable. Greenish light gray marl and greenish light gray siltstones.	Resevoir and Source
SU2		early Aptian	4330	~1900	14206	~6234	Synrift	Low-amplitude and high frequency in the upper part, and moderate to high-amplitude in the lower part.	Greenish light gray siltstone, semihard to hard. Whitenish gray sandstone, very fine to medium, subrounded to subangular, well to moderately sorted, composed of quartz, matrix composed of kaolinite, slightly micritic, porosity between 0 and 15%, friable to semifriable. Reddish brown shales, and dark gray shales, semihard.	Resevoir (?) and Source
SU1	?		~6230	?	~20440	?		Moderate to high-amplitude reflectors in upper part, and low to moderate-amplitude reflectors in lower part.	?	Resevoir (?) and Source (?)

obs: Without return of samples between 2158 and 2907 m. Lithology was interpreted based on seismic data, drilling parameters and LWD profiles (Logging While Drilling).

Legend: Sandstone · Siltstone · Mudstone · Shale · Calcilutite · Marl

Figure 6. Lithostratigraphy at the Pecém well and correlative seismic facies and units. The internal character, geometry, and terminations of SU1 to SU7 are described in detail. MD = measured depth; obs = observation.

the late Aptian. In addition, SU1, SU2, and SU3 are cut by high-angle normal faults. Divergent throws and dips offset SU1 and SU2, forming an asymmetric graben (minibasin) filled by SU3 (Figures 7B, 8F).

The SU3 comprises the Paracuru Formation, which, in deep waters is composed of thin intercalations of sandstone, siltstone, shales, and marls, filling fault-bounded depocenters in the area around Pecém well (Figures 5, 6). This sequence becomes thinner toward the most distal part of the margin (Figure 4).

A magmatic intrusion is observed at the top of SU3 (Figure 8E). This intrusion has a parabolic shape and its internal reflections are chaotic (Figure 8E).

Seismic Unit 4: Upper Aptian to Near-Top Cretaceous (Transgressive Drift Sequence)

The SU4 shows transparent to parallel internal reflections, the latter of which are continuous and of low amplitude. An abrupt change exists in the petrophysical character between SU3 and SU4 when considering the GR and acoustic slowness curves (DT). The GR values decrease sharply in SU4 (mean GR values in SU4 = 30 API; mean GR values in SU3 = 85 API), together with sonic traveltime (mean acoustic slowness in mean acoustic slowness in SU4 = 125 μs/ft (410 μs/m); mean acoustic slowness for SU3 = 90 μs/ft (295 μs/m) (Figures 3, 5J).

The SU4 is the first sequence in deep-water that is not significantly affected by faulting, and fills the hanging-wall depocenter in Figure 5. Its lower boundary is an upper Aptian regional unconformity. Along this same boundary, there are multiple incision surfaces (Figure 9B) and an angular unconformity is observed between SU4 and SU3 (Figure 5B).

These features, and the sharp change in GR and sonic traveltime across this same unconformity indicate a regional erosional event. The onlapping reflections observed in Figure 5B indicate that SU4 comprises a transgressive sequence marked by the deposition of marine calcareous shale with very thin intercalations of sandstones, marls, and calcilutites (Figure 6).

The SU4 comprises the Uruburetama Member of the Ubarana Formation (Figure 3).

Seismic Unit 5: Near-Top Cretaceous to Upper Oligocene (Regressive Drift Sequence I)

The lower boundary of SU5 (horizon 4) is a high-amplitude continuous horizon. The SU5 is locally transparent with prograding and subparallel low-amplitude internal reflections (Figure 3). It is locally deformed by closely spaced normal faults (Figure 5C). Lithologically, SU5 is composed of thin intercalations of marls, calcilutites, and shales (Figure 6).

The SU5, SU6, and SU7 comprise the Itapajé Member of the Ubarana Formation (Figure 3).

Seismic Unit 6: Upper Oligocene to Intra-Miocene (Regressive Drift Sequence II)

The lower boundary of SU6 is marked by an erosional unconformity. The SU6 is composed of prograding high-amplitude reflections and its internal character is chaotic to continuous (Figures 3, 5, 8). The SU6 is mainly composed of marls with minor intercalations of shales, sandstones, and calcilutites (Figure 6).

Seismic Unit 7: Intra-Miocene to Miocene (Transgressive Drift Sequence)

This unit is shown as an alternating succession of chaotic to continuous, low- to medium-amplitude seismic reflections of high frequency (Figures 3, 5, 6). The SU7 comprises plastered deposits on the continental rise, which are slope-elongated and characterized by their high-amplitude seismic reflections with hummocky and wavy reflectors (Figures 4, 5E, 8). Therefore, these deposits are interpreted as contourites (Faugères et al., 1999). They are crossed by furrows and submarine canyons. Transgressive seismic configurations are observed on Figure 5.

Submarine creep movements also occur in the deep-water Mundaú subbasin. Listric faults may root into the basal gliding planes responsible for these creep movements (Figures 5F, 8C).

Lithologically, SU7 is composed of marls, shales, mudstones, and calcilutites (Figures 3, 5, 6).

Petroleum System

Source Rocks

Table 2 presents the values of percentage of TOC (TOC%) and Rock-Eval pyrolysis obtained for the shales of the Ubarana, Paracuru, and Mundaú Formations in the Pecém well. Their TOC content ranges from 0.46% to 4.19%. In general, a value of approximately 1% TOC is considered a minimum

Figure 7. Southwest-northeast seismic section. Vertical scale in two-way traveltime (milliseconds). (A) Location of the selected seismic section. (B) Normal faults with divergent throws and dips, forming a small subbasin in seismic unit 1 (SU1), SU2 and SU3 (synrift and transitional sequences). (C) Faults in the postrift SU7. (D) Upper Oligocene, reactivated negative flower structure (interpreted and noninterpreted data). (E) High-amplitude reflectors in SU1. Vertical exaggeration (Z) is 3 in (A) and 5 in (B)–(E).

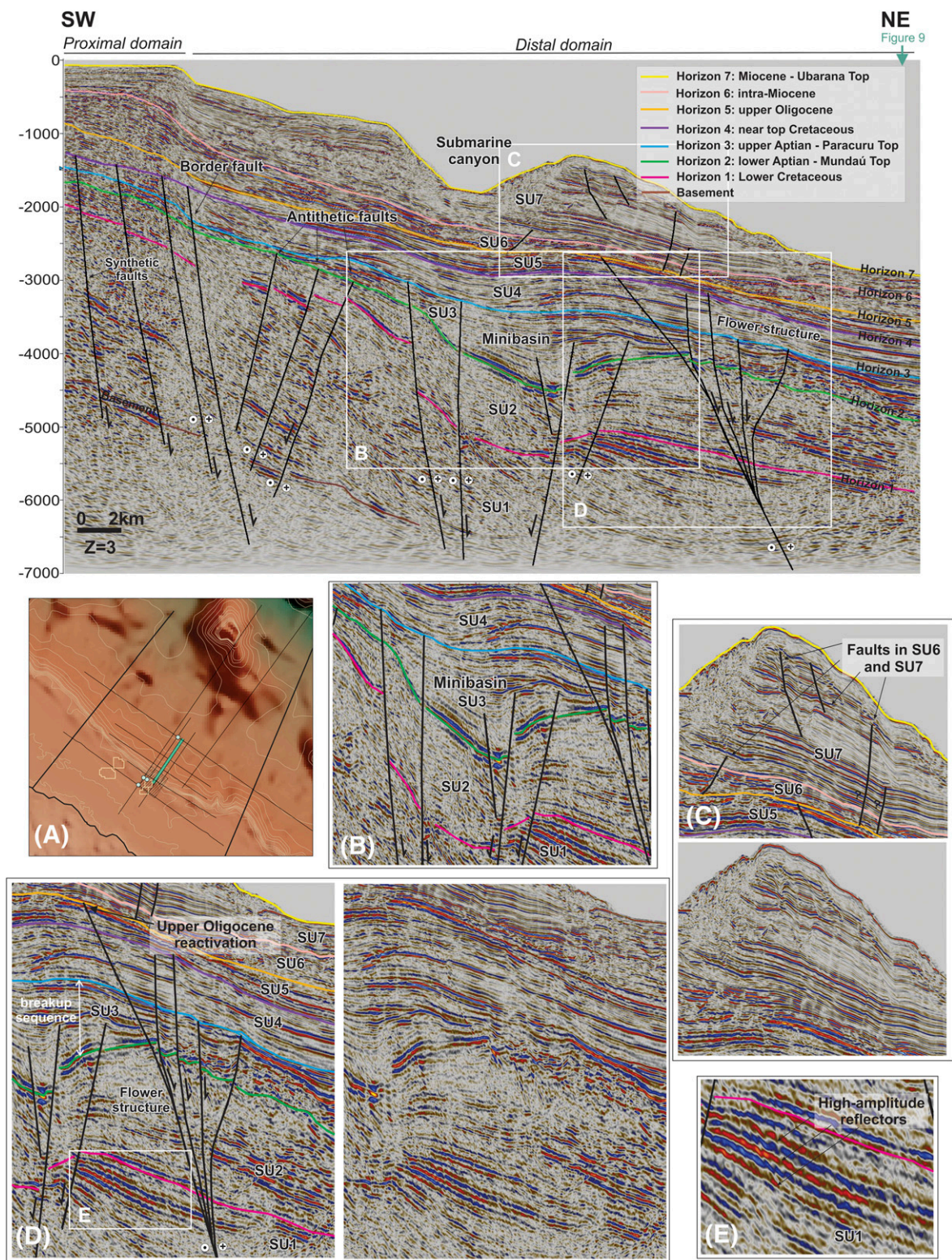**808**   Evolution and Petroleum Systems of Deep-Water Mundaú Subbasin
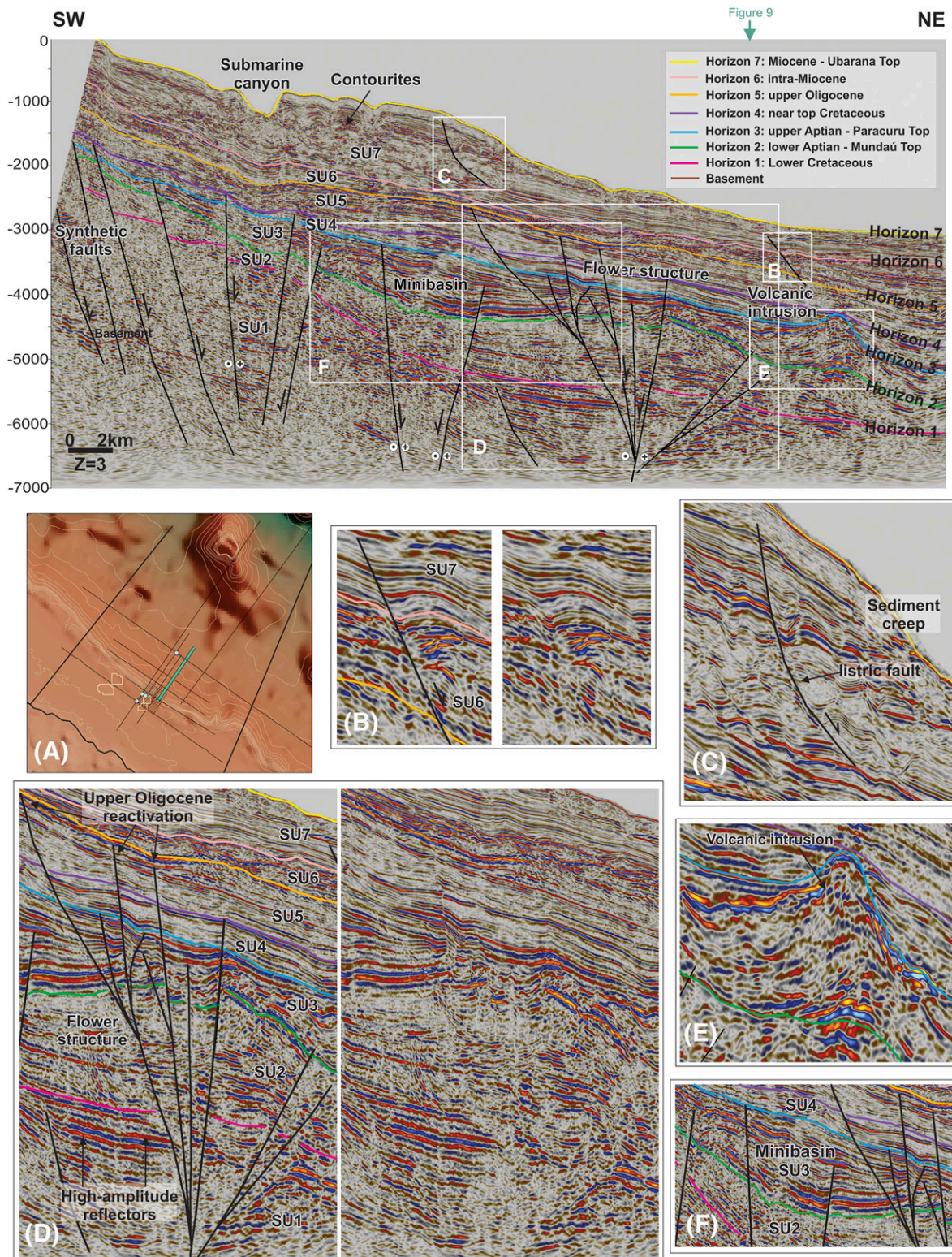
Figure 8. Southwest-northeast seismic section. Vertical scale in two-way traveltime (milliseconds). (A) Location of the seismic section. (B) Fault in postrift sequences (seismic unit 6 [SU6] and SU7). (C) Sediment creep in SU7. (D) Upper Oligocene reactivated flower structure (interpreted and noninterpreted data) and high-amplitude seismic reflectors in SU1. (E) Volcanic intrusion in SU3. (F) Minibasin filled by SU3. Vertical exaggeration (*Z*) is 3 in (A) and 5 in (B)–(F).

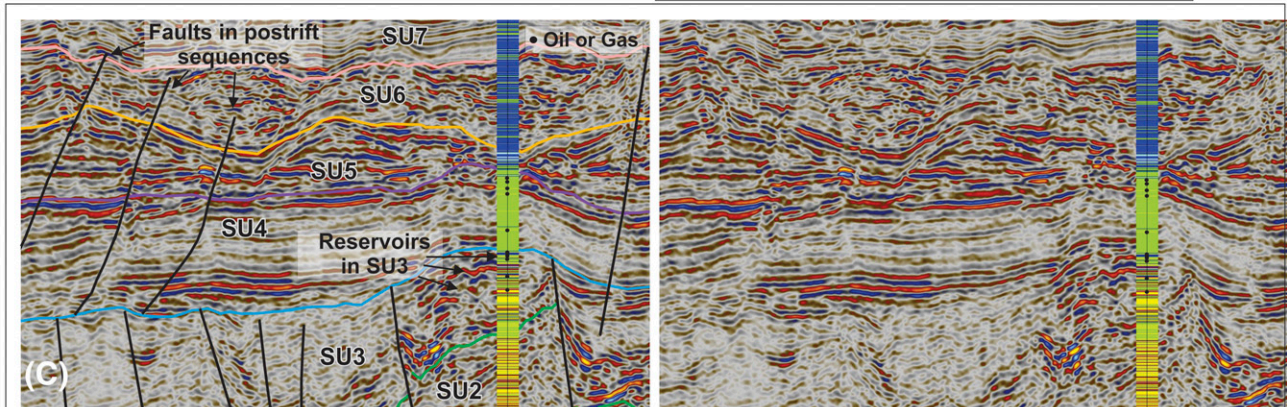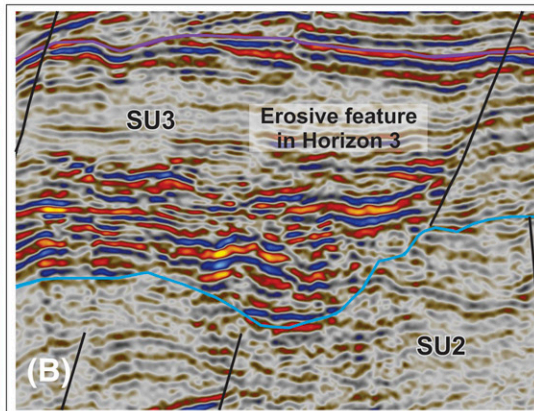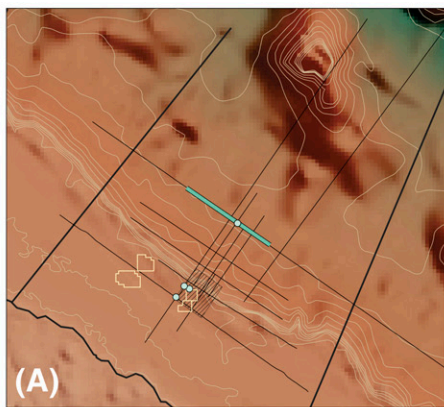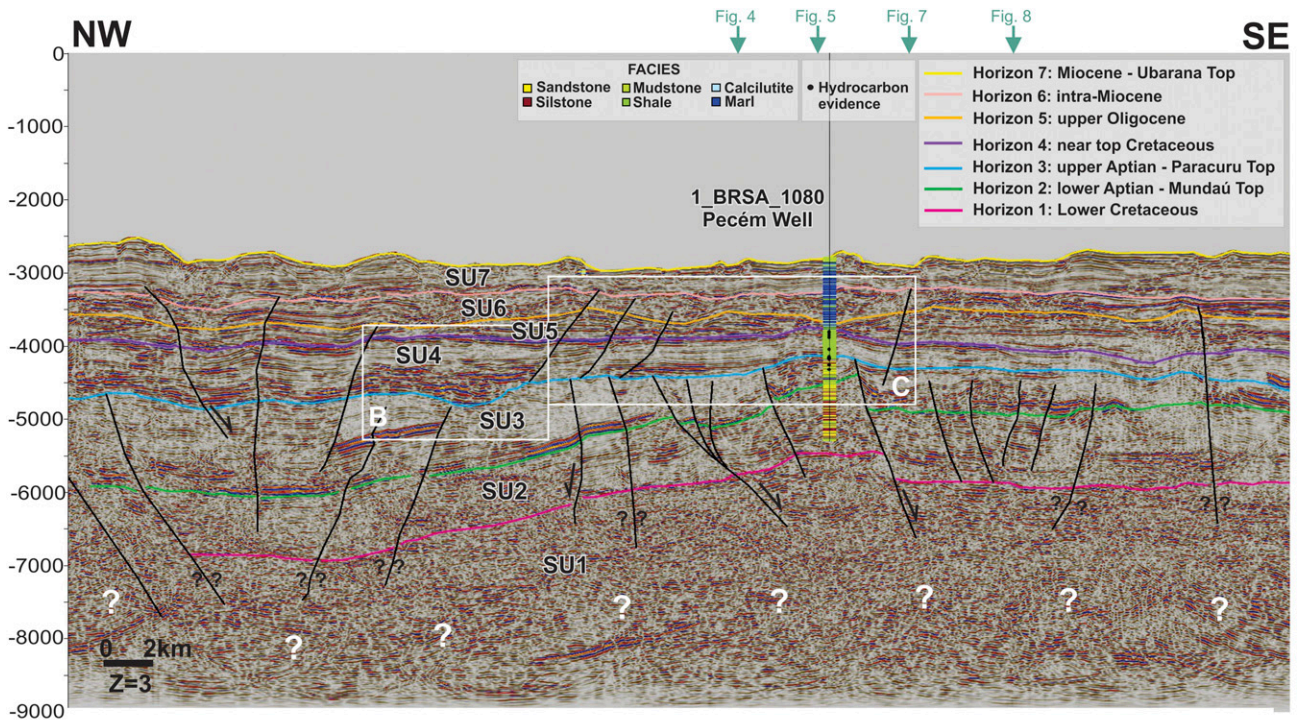**Figure 9.** Northwest-southeast seismic section showing the Pecém well over a raised tilt block limited by faults. Vertical scale in two-way traveltime (milliseconds). (A) Location of the seismic section. (B) Erosive feature in horizon 3. (C) Reservoirs in seismic unit 3 (SU3) and SU4. Faults in postrift strata. Vertical exaggeration (Z) is 3 in (A) and 5 in (B) and (C).

Table 2. Total Organic Carbon and Rock-Eval Pyrolysis Data for Mundaú, Paracuru, and Ubarana Source Rocks in Well 1_BRSA_1080 (Pecém Well)

Sample	Sample Type	Sample Top, m	Sample Top, ft	SU	Formation	TOC, wt. %	Insoluble Residue, %	S_1, mg HC/g Rock	S_2, mg HC/g Rock	S_3, mg CO$_2$/g Rock	S_1/TOC	PI	T_{max}, °C	Hydrogen Index, mg HC/g TOC	Oxygen Index, mg CO$_2$/g TOC
1	Lateral sample (rock)	3607	11,834	SU4	Ubarana	3.63	90	1.74	15.02	0.16	0.48	0.10	425	413.8	4.4
2	Lateral sample (rock)	3676	12,060	SU4	Ubarana	4.19	90	7.55	18.93	0.31	1.80	0.29	424	451.8	7.4
3	Lateral sample (rock)	3903	12,805	SU3	Paracuru	3.56	79	3.24	13.61	0.7	0.91	0.19	439	382.3	19.7
4	Fluid sample (rock)	4050	13,287	SU3	Paracuru	1.17	83	0.86	3.63	0.81	0.74	0.19	449	310.3	69.2
5	Fluid sample (rock)	4266	13,996	SU3	Paracuru	1.16	83	0.56	3.15	0.74	0.48	0.15	446	271.6	63.8
6	Fluid sample (rock)	4374	14,350	SU2	Mundaú	0.68	85	0.56	2.42	0.45	0.82	0.19	441	355.9	66.2
7	Fluid sample (rock)	4803	15,758	SU2	Mundaú	0.46	90	–	–	–	–	–	–	–	–
8	Fluid sample (rock)	5376	17,638	SU2	Mundaú	0.49	88	–	–	–	–	–	–	–	–
9	Fluid sample (rock)	5616	18,425	SU2	Mundaú	0.93	86	0.64	3.57	0.68	0.69	0.15	442	383.9	73.1
10	Fluid sample (rock)	5826	19,114	SU2	Mundaú	0.78	90	0.5	5.03	0.47	0.64	0.09	442	644.9	60.3
11	Fluid sample (rock)	5874	19,272	SU2	Mundaú	1.38	89	0.79	6.35	0.51	0.57	0.11	442	460.1	37.0
12	Fluid sample (rock)	5913	19,400	SU2	Mundaú	1.97	89	0.83	9.16	0.52	0.42	0.08	442	465.0	26.4

Hydrogen index is the ratio between S_2 and TOC ($HI = [S_2/TOC] \times 100$ in milligrams of HC per gram of TOC), oxygen index is the ratio between S_3 and TOC ($OI = [S_3/TOC] \times 100$ in milligrams of CO$_2$ per gram of TOC), and production index is the ratio of the amount of free hydrocarbons already generated, compared with the total amount of hydrocarbon that rocks can generate ($PI = S_1/(S_1 + S_2)$). Only samples displaying a TOC content of approximately 1% were submitted to Rock-Eval pyrolysis analyses. All others are indicated by a dash.

Abbreviations: HI = hydrogen index; OI = oxygen index; PI = production index; S_1 = the amount of free hydrocarbons present in the sample before the analysis (milligrams of HC per gram of rock); S_2 = the amount of hydrocarbons that formed during thermal pyrolysis (milligrams of HC per gram of rock); S_3 = the CO$_2$ yield during thermal breakdown of kerogen (milligrams of CO$_2$ per gram of rock); SU = seismic unit; T_{max} = maximum temperature recorded at the maximum of hydrocarbon generation during pyrolysis (degrees Celsius); TOC = organic carbon content (weight percent).

MAIA DE ALMEIDA ET AL.   **811**

value to form an effective source rock. The vertical distribution of our results shows, from a stratigraphic point of view, seven samples with values above 1% (1–5, 11, and 12; Table 2).

Hydrocarbon Potential

The TOC% values for source rocks in the Mundaú Formation (SU1 and SU2) are between 0.46% and 1.97%, indicating poor to good source potential (Tables 1, 2). However, Peters and Cassa (1994) point out that TOC by itself is not always a good indicator of source rock potential because measurements may include inert carbon that has little or no generating potential. The two aforementioned authors believe that the S_2 measurement derived from pyrolysis analysis is a better indicator of the generation potential of source rocks. The plot of TOC versus S_2 was established to get an idea about the quantity of organic matter present and its associated hydrogen. The data shown in Figure 10A indicates that the Mundaú Formation samples represent fair to good generation potential.

In the Paracuru Formation (SU3), TOC% values are between 1.16% and 3.56%, indicating good to very good amounts of organic matter (Table 1) and good to very good generation potential (Figure 10A).

For source rocks in the Ubarana Formation (SU4), TOC% values vary between 3.63% and 4.19%, indicating very good to excellent source rocks (Tables 1–5) with a very good hydrocarbon generation potential.

Analyzed samples from the Mundaú Formation are composed of dark to reddish-brown shales, whereas samples in the Paracuru and Ubarana Formations are composed of greenish, dark to light gray carbonaceous shale (Figure 6).

According to the S_2 parameter on Rock-Eval tests, and the classification of Espitalié et al. (1977) (Table 1), the Mundaú Formation presents moderate to good potential as a source interval (Table 2). The Paracuru Formation presents good to excellent potential and the Ubarana Formation displays excellent potential.

Organic Matter Type

The HI shows that most samples are potential oil generators (Tables 1, 2), except for one sample in the Paracuru Formation showing potential for gas and condensate.

On a graph of HI versus OI (van Krevelen, 1961), most of the samples plot in the field of type II kerogen (Figure 10B). Type II kerogen is a mechanically and chemically complex mixture of algae, marine organisms, and plant debris. This is the usual type of kerogen found in marine basins where mixtures of phytoplankton, zooplankton, and microorganisms have accumulated under reducing conditions, commonly containing land-derived plant material (Bjørlykke, 2010).

Thermal Maturity

To assess the maturity samples taken from the deep-water Pecém well, the data obtained were plotted on a HI versus T_{max} diagram (Figure 10C). According to Peters (1986) and Espitalié et al. (1977, 1985), oil generation from source rocks begins at T_{max} = 435°C –465°C, which means that the Mundaú and Paracuru Formations are within the oil window (type II kerogen). The source rocks of these formations are thermally (early) mature (T_{max} values range from 439°C to 449°C). However, the samples from the Ubarana Formation are considered thermally immature (T_{max} ranges from 424°C to 425°C) (Figure 10C; Table 2), not reaching sufficient maturity to generate hydrocarbons.

The PI confirms that most samples are mature (oil generation) because PI ranges from 0.10 to 0.29 (Tables 1, 2), except for two samples from the Mundaú Formation, whose PI values are 0.08 and 0.09 (immature).

Durand (1988) stated that the expulsion (or primary migration) of hydrocarbons from source rocks toward their reservoir(s) is the first migration stage for organic material after its transformation into petroleum. Smith (1994) and Hunt (1996) determined that the ratio of S_1 to TOC should be between 0.1 and 0.2 for oil expulsion to start in the source rock. Table 1 shows that the S_1/TOC ratios for all the samples are higher than 0.1. The values range from 0.42 to 1.80. Hence, these results indicate that these source rocks are able to expel hydrocarbons.

A plot of S_1 versus TOC (Figure 10D; Table 2) was used to discriminate nonindigenous (allochthonous) from indigenous hydrocarbons (autochthonous) (Peters, 1986; Hunt, 1996; Rabbani and Kamali, 2005). The graph distinguishes between migrated
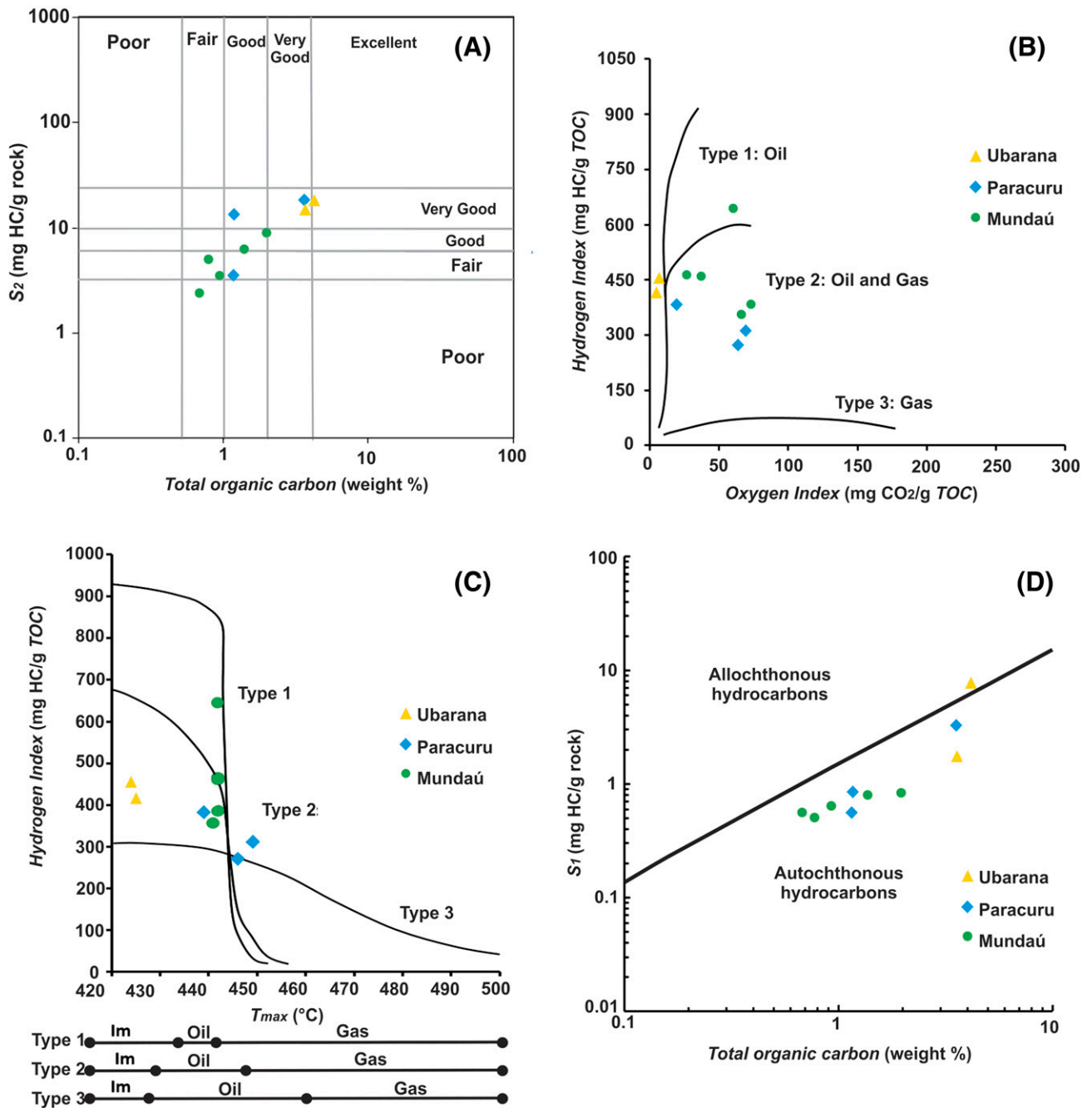
Figure 10. (A) Plot of total organic carbon (*TOC*) versus residual hydrocarbon potential (S_2) showing source rock generation potential. (B) Modified Van Krevelen diagram showing the primary composition of source rocks in the Pecém well. (C) Hydrogen index versus maximum temperature recorded at the maximum of hydrocarbon generation during pyrolysis (T_{max}) showing the maturity of organic matter. Im = immature. (D) Diagram of S_1 versus *TOC* to discriminate between nonindigenous (allochthonous) and indigenous (autochthonous) hydrocarbons in the Pecém well.

hydrocarbons and contaminants from autochthonous hydrocarbons. The dividing line in the plot (Figure 10D) is where $S_1/TOC = 1.5$ (Hunt, 1996; Rabbani and Kamali, 2005; El Nady et al., 2015). Values belonging to allochthonous hydrocarbons appear above this line, whereas autochthonous

hydrocarbon values emerge below it. In the study area, most of the samples are classified as autochthonous hydrocarbons (Figure 10D). This indicates that oil has not migrated from a distant source rock. In essence, they were accumulated very close to their source. Only one sample is considered

here to represent allochthonous hydrocarbons (Ubarana Formation, Figure 10D).

It is noted here that the deepest sample analyzed was taken at 5913 m (19,400 ft). The possibility of source rocks at depths greater than 5913 m (19,400 ft), putatively related to the onset of rifting on the BEM, cannot be ruled out (see the Discussion section).

Reservoir Rocks

Reservoir intervals in the deep-water Mundaú subbasin are chiefly siliciclastic. They comprise very thin intercalations of sandstone, shale, siltstone, and marls (Figure 6). Hydrocarbons were found in fluid samples and by gas detectors in several intervals (Figures 5H, 9C; Table 3). The sandstone layers forming reservoir intervals in the Pecém well are approximately 1-m (~3.28-ft) thick near the top of Paracuru Formation (SU3). However, as the depth increases, the thickness of sandstone layers also increases, reaching 10 m (32.8 ft) in some intervals (Figures 5H, 9C).

The main reservoir rock in the Paracuru Formation is composed of brownish subangular sandstone. Its grain size ranges from very fine to medium sand and is well sorted. It consists of quartz and micritic sandstone and its matrix can be sandy, silty, or clayey. Porosity ranges from 0% to 15%. It is semifriable to friable, sometimes with carbonaceous clasts. These sandstones are locally stained by dark brownish oil. Layers of dark clay shales are found in contact with these sandstones (Figures 5H, 6, 9C).

Well tests from the Pecém well were promising (Figure 2; Table 3). The test in the interval between 3800 and 3818 m (12,467.2 and 12,526.3 ft) indicated that it is an oil-bearing overpressured interval. The test was carried out after a stimulation operation with hydraulic fracturing. Before the fracturing operation, the interval was perforated. The oil is 30° API, the flow rate is 90 m^3/day (3178.32 ft^3/day), the transmissibility is 7.9 md.m/cP, and the maximum temperature registered was 87.3°C. Other intervals in the Paracuru Formation also had effective well tests at depths between 3880–3913 m (12,730–12,838 ft) and 4016–4178 m (13,176–13,707 ft).

Gas shows were found in the Uruburetama Member of the Ubarana Formation. The reservoirs in this member comprise very thin layers of sandstone and calcilutite (Figures 5, 9C). However, well tests were not favorable at this stratigraphic level (Table 3).

The well-test failures were attributed to poor seal competence.

Seal Units

The main seal unit in the distal domain is the transgressive, shaley Uruburetama Member of the Ubarana Formation (SU4) (Figures 5, 6, 9). It comprises semihard light to dark gray shales, greenish, and carbonaceous. These shales are thinly intercalated by light gray marls and very fine to fine hyaline sandstones, forming a 607-m (1991.47-ft)-thick unit (Figure 6). It is also worth mentioning the existence of intraformational shales that are important seal intervals in the Paracuru Formation (Figures 5, 6, 9).

Trap Formation and Migration of Hydrocarbons

The main trapping style in deep-water Mundaú subbasin is a mixed structural–stratigraphic trap comprising a normal fault and an erosional unconformity. An upper Aptian oceanward-dipping fault is responsible for the trap because it places Aptian rocks of the Paracuru Formation (SU3) in direct contact with the near-top Cretaceous transgressive marine shales of the Uruburetama Member (SU4). Reservoirs are located on the footwall of this normal fault (Figures 5H, J; 9C).

It is worth pointing out that gas was also found in local stratigraphic traps at the top of Uruburetama Member (horizon 4, near-top Cretaceous) (Figures 5, 9C). Here, the stratigraphic traps consist of sandstone and calcilutites layers intercalated between shales. Considering that the Uruburetama Member is immature (Figure 10C), gas likely migrated from a deep mature source rock after the trap was formed. Thus, it is estimated that the migration occurred in the Cenozoic because the trap was completely formed near-top Cretaceous (horizon 4). Integrated studies using geothermal and geochemical data should be performed to evaluate when exactly the maturation and migration happened in the study area.

Hydrocarbon migration may have occurred in two distinct ways in the deep-water Mundaú subbasin: (1) through direct flow of hydrocarbon-rich (source) shales juxtaposed with reservoir intervals, or (2) by migration along faults and unconformity traps. The regional unconformity topping the Paracuru Formation may have been an important pathway for hydrocarbon migration because the reservoir

Table 3. Intervals with Oil or Gas Shows and where Well Tests Were Undertaken in the Pecém Well

Formation	Interval, m (ft)		Hydrocarbon Evidence Type[†]	Gas Detector[‡]		Well Test[§]	Static Pressure, MPa (psi)[¶]
	Top	Base*		Total Gas	Heavy Gas		
Ubarana	3194 (10,479)	3197 (10,489)	Gas detector	18.0	0.4	–	–
Fm. (SU4)	3217 (10,554)	3229 (10,594)	Gas detector	22.0	0.4	–	–
	3249 (10,659)	3254 (10,676)	Gas detector	22.3	0.4	–	–
	3272 (10,735)	3288 (10,787)	Gas detector	18.3	0.5	–	–
	3424 (11,234)	3436 (11,273)	Gas detector	20.6	0.4	–	–
	3539 (11,611)	3542 (11,621)	Gas detector	7.0	0.1	No seal	–
	3551 (11,650)	3553 (11,657)	Gas detector	9.0	0.1	–	–
	3568 (11,706)	3570 (11,713)	Gas detector	14.3	0.2	No seal	–
	3584 (11,759)	3587 (11,768)	Gas detector	10.8	0.4	–	–
	3591 (11,781)	3596 (11,798)	Gas detector	15.5	0.3	No seal	–
	3644 (11,955)	3647 (11,965)	Gas detector	24.9	0.5	–	–
	3654 (11,988)	3660 (12,008)	Gas detector	33.6	0.7	–	–
	3666 (12,028)	3671 (12,044)	Gas detector	35.4	0.9	No seal	–
Paracuru	3770 (12,369)	3770 (12,369)	Fluid sample	–	–	–	–
Fm. (SU3)	3774 (12,382)	3774 (12,382)	Fluid sample	–	–	–	–
	3797 (12,457)	3798 (12,461)	Gas detector	46.9	1.7	–	–
	3802 (12,474)	3804 (12,480)	Gas detector	53.9	1.4	Effective	625 (90,666)
	3811 (12,503)	3811 (12,503)	–	–	–	Effective	628 (91,110)
	3819 (12,528)	3819 (12,528)	–	–	–	Effective	629 (91,250)
	3842 (12,605)	3842 (12,605)	Fluid sample	–	–	Closed	–
	3845 (12,613)	3845 (12,613)	Fluid sample	–	–	No seal	–
	3845 (12,615)	3845 (12,615)	–	–	–	Effective	632 (91,706)
	3880 (12,730)	3880 (12,730)	Fluid sample	–	–	Effective	640 (92,838)
	3889 (12,760)	3889 (12,760)	–	–	–	Effective	641 (92,935)
	3890 (12,762)	3890 (12,762)	–	–	–	Effective	640 (92,872)
	3913 (12,838)	3913 (12,838)	–	–	–	Effective	644 (93,474)
	4016 (13,176)	4016 (13,176)	–	–	–	Effective	666 (96,526)
	4147 (13,606)	4147 (13,606)	–	–	–	Effective	691 (100,223)
	4178 (13,707)	–	–	–	–	Effective	700 (101,497)

Abbreviations: Fm. = Formation; SU = seismic unit.
*Dash indicates unknown depth.
[†]Dash indicates no hydrocarbon evidence.
[‡]Dash indicates no gas detection.
[§]Dash indicates no well test undertaken.
[¶]Dash indicates no information about static pressure.

interval is largely located in the upper part of this formation (Figures 5H, J; 9C).

DISCUSSION

Tectonic Evolution of the Deep-Water Mundaú Subbasin, Ceará Basin

Three main domains were interpreted in the Mundaú subbasin based on this work: proximal, distal, and RFZ domains (Figure 4). The proximal domain is characterized by large extensional faults on the continental shelf that bound multiple half grabens (Figure 4B). This domain occurs at water depths between 30 and 60 m (98.4 and 196.9 ft) and shows growth strata adjacent to oceanward-dipping, synthetic normal faults (Figure 4). These oceanward-dipping faults present a mean distance from each other of approximately 2 km (~6562 ft). The dip on successively younger strata diminishes, indicating growth in the

Aptian. The landward dip of horizon 1 is approximately 15°, whereas horizon 3 is almost flat (Figure 4).

The latter faults sole out in the basement and were active until the late Aptian. Some of them continued moving into the Late Cretaceous (early drift stage) (Figure 4B). Many of these faults have geometries that indicate strike-slip motion, such as near-vertical dip, changes in fault throw with depth, abrupt changes in seismic character and strata thickness across the fault (Figure 4).

The distal domain on the continental slope is characterized by high-angle landward-dipping rollover faults that affect the synrift and transitional sequences (SU1, SU2, and SU3) (Figures 4, 5, 7–9). Rollover faults comprise normal faults generated on top of monoclinal rollovers and turtle anticlines (Rowan et al., 1999). On the continental rise and abyssal plain, high-angle landward- and oceanward-dipping faults occur. The spacing between the faults ranges from 800 to 3000 m (2625 to 9843 ft). Similarly to the proximal domain, some of these faults present geometries that are typical of transtensional structures, such as near-vertical dip, abrupt changes in seismic character, and sharp differences in strata thickness across faults (Figure 5G).

Transtensional deformation caused by the opening of the equatorial Atlantic Ocean, and acting on second- and third-order transform faults between the RFZ and the CFZ, produced depocenters limited by faults with divergent throws and dips (Figures 7B, 8F). These minibasins provided additional accommodation space for the transitional SU3 (Figure 7B).

Our seismic interpretation shows that faults in the distal domain, in general, sole out around horizon 3 (upper Aptian). However, some faults appear to be younger than the Aptian. Late Oligocene reactivation of flower structures is shown in Figures 7D and 8D. In addition, other faults were shown to crosscut SU4, SU5, and SU6, indicating local faulting during the drift stage (Figures 5C, 7C, 8B, 9C). The SU7 is also cut by oceanward-dipping listric faults that are rooted on shallow glide planes accommodating submarine creep movements (Figures 5F, 8C).

The RFZ domain is characterized by subvertical faults and a volcanic seamount (or guyot), the Canopus Bank (Figures 2, 4), formed under the direct influence of the RFZ. The internal character of the seamount is mainly chaotic (Figure 4).

The Canopus Bank is a north-northwest–trending intrusion, 80 km (47.71 mi) long, 40 km (24.85 mi) wide, covering an area approximately 2500 km^2 (~965.26 mi^2). Its top reaches a water depth of 150 m (492 ft) and is approximately 120 km^2 (~46.3 mi^2) in area.

Parallel, subhorizontal seismic reflections on the Canopus Bank are interpreted as pelagic and hemipelagic strata. The present-day morphology of the seamount suggests that magmatic activity has ceased for several million years; depositional processes predominate over the seamount as demonstrated by a sequence of subparallel reflections on its top (e.g., Jovane et al., 2016) (Figure 4). It is interpreted that the magmatism in this region has been inactive since, at least, the late Oligocene (ca. 23 Ma) because horizon 5 tops the Canopus Bank. Taking into account that this magmatic intrusive event cuts across horizon 4 (near-top Cretaceous; ca. 65 Ma), and the inclined internal reflections in SU1 to SU4 (Figure 4D), we conclude that the intrusive event occurred after the Cretaceous. If the intrusive event had happened before this time, the SU1 to SU4 reflections should be parallel and horizontal, not inclined. Thus, estimates of the timing of the volcanic emplacement range between 65 and 23 Ma. In addition, the hypothesis of seamount building because of multiple magmatic events is not disregarded. Various sea-floor multiples were found in the seismic data and prevented a better interpretation of this part of the study area.

In regional seismic profiles (Figure 4), our interpretation favors thick continental crust in the proximal domain (continental shelf) and thin continental crust in the distal domain (continental slope and continental rise). The transition from sedimentary sequences to the continental crust is marked by a high-reflectivity zone at a depth of 7000–8000 ms twt (Figure 4).

A conceptual model for the evolution of the deep-water Mundaú subbasin is shown in Figure 11. Here, the models from Mascle and Blarez (1987) and Mercier de Lépinay et al. (2016) were modified by adding a transitional stage and adopting the terms prerift, synrift, transitional, and drift stages instead of pretransform, syntransform, and posttransform. These stages are discussed as follows.

The prerift stage (stage A in Figure 11) is characterized by an active continent to continent contact (Mascle and Blarez, 1987), when the Transbrasiliano lineament and the Kandi Fault Zone were still connected in a northeast-southwest direction (Pankhurst et al., 2008; Moulin et al., 2010). Although there are no known prerift sedimentary rocks in the Ceará Basin, they exist on its conjugate margin (Figure 11). The lower part of the Ise Formation, in the Benin Basin, is Upper Jurassic. Additionally, the Sekondi Formation, in the Keta Basin, may correlate to the Upper Jurassic Ise Formation (Elvsborg and Dalode, 1985). They represent the uppermost part of the prerift stage on the conjugate margin.

The synrift stage is characterized by an active margin-to-margin contact (Mascle and Blarez, 1987). During this stage, transtensional stresses created northwest-southeast en echelon depocenters (Matos, 1999), and the Ceará Basin was limited by the RFZ and CFZ (Figure 11). In the deep-water Mundaú subbasin, the synrift stage is subdivided into two stages.

Synrift stage 1 (stage B in Figure 11) is characterized by the generation of wide faults bounding half grabens (Figure 11).

At present, no strata older than the early Aptian have been sampled in the Ceará Basin. However, older synrift strata are present in the basin as indicated by the thick seismic packages imaged in this work (Figure 4). This package suggests the presence of synrift strata of Berriasian age, equivalent to the Pendência Formation in the Potiguar Basin, deposited in lacustrine, fluvio-deltaic, and fan-deltaic environments (Pessoa Neto et al., 2007).

This stage is characterized by generation of oceanward-dipping faults in the proximal domain and landward- and oceanward-dipping faults in the distal domain (Figure 11). All faults created large amounts of sediment accommodation space in basins generated between tectonically active tilt blocks. These faults continued to evolve into the next stage.

Synrift stage 2 (stage C in Figure 11) is characterized by the deposition of SU2 during the early Aptian. There is a continuous increase in lithospheric extension as marked by the continuous vertical propagation of the older faults. The basin sedimentary cover was progressively deformed (Figure 11).

The transitional stage (stage D in Figure 11) is characterized by an upper Aptian breakup sequence (SU3), correlating with the Paracuru Formation, which contains the main reservoir interval of the Mundaú subbasin (see Soares et al., 2012; Alves and Cunha, 2018). Horizon 2 marks the base of SU3 and it indicates the onset of the lithospheric breakup between the BEM and West African margin. It separates continental depositional environments from transitional and typically marine depositional environments above (Figures 3, 6).

The lithospheric breakup event is thus associated with a discrete sedimentary sequence (breakup sequence) of regional extent. The faulted sequence SU3 records the transitional period spanning from the onset of the lithospheric breakup event to the establishment of thermal relaxation as the main control on subsidence of the continental margin (Soares et al., 2012).

The angular unconformity and the sharp contact at the top of the SU3 indicate widespread erosion at the end of the transitional stage (Figures 3; 5B, J; 9B).

During the transitional stage, flower structures propagated farther (Figures 7D, 8D, 9), indicating that the deep-water Mundaú subbasin developed as a transtensional system. At the end of this stage, the mid-Atlantic spreading center was responsible for the inception of the drift stage.

In the drift stage (stages E and F in Figure 11), the transform contact was active between two areas of oceanic crust. Hence, an oceanic fracture zone was created. The continental margin was directly placed adjacent to hot (but progressively cooling) oceanic crust (Mascle and Blarez, 1987).

The drift stage in the distal Mundaú subbasin started in the Late Cretaceous. First, transgressive deep-marine shales were deposited (SU4), followed by the accumulation of regressive sequences (SU5 and SU6) composed of marls, calcilutites, shales, and mudstones. The transgressive sequence SU7 comprises plastered and wavy reflections, which were interpreted as contourites. Submarine canyons eroded the sea floor.

Short submarine creep movements were mapped highlighting the local importance of gravity tectonics in the study area (Figures 5F, 7C, 8C). Regional-scale gravitational systems occur in other basins of the BEM such as in Foz do Amazonas (Silva et al., 1998; Cobbold et al., 2004; Reis et al., 2010, 2016), Pará-Maranhão, and Barreirinhas (Oliveira et al., 2012), but they were not found in the Mundaú subbasin. Silva et al. (1998) proposed some ideal conditions for the development of these gravity tectonics. Clastic sediments bypass the shelf edge through submarine
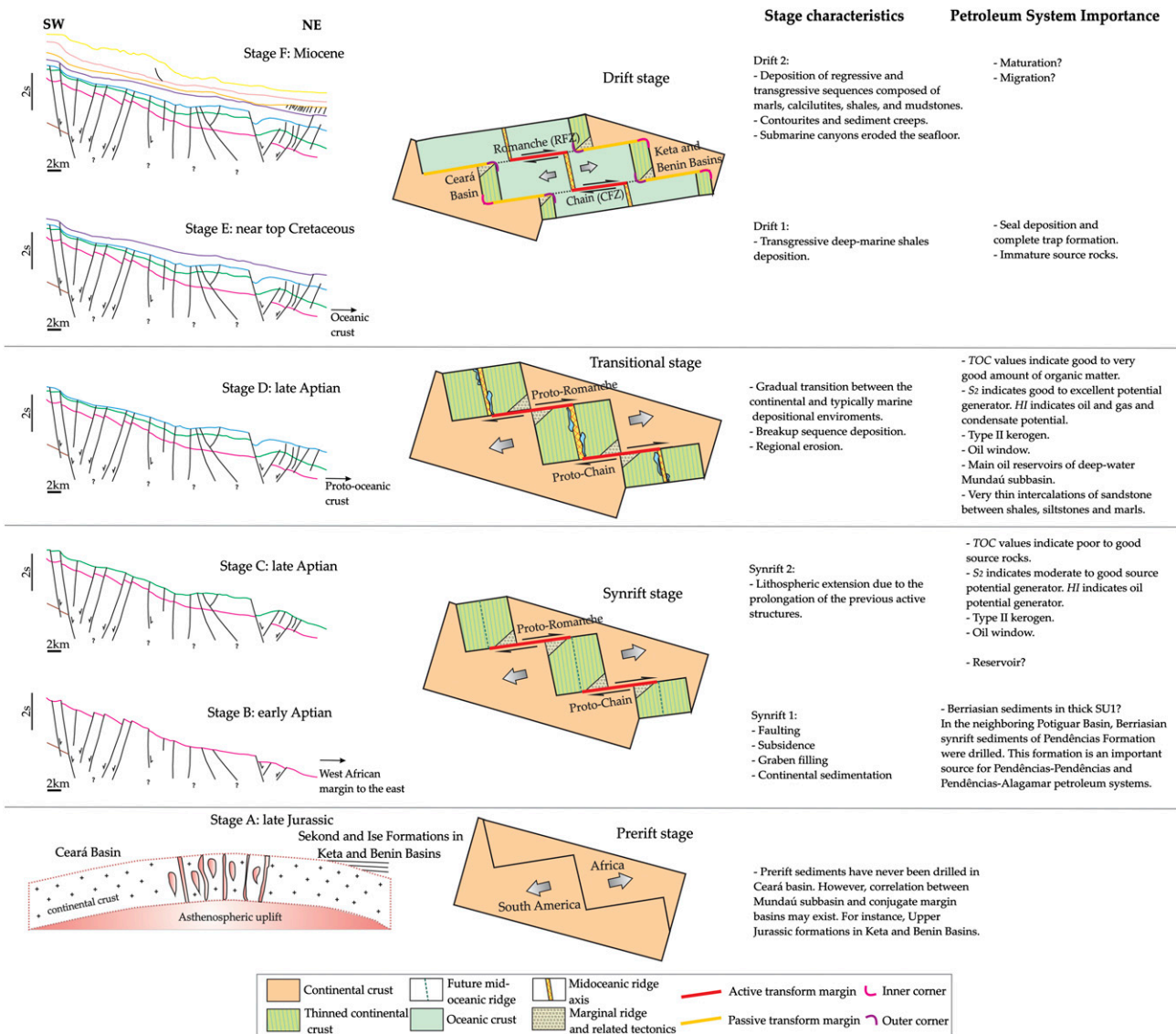
Figure 11. Diagram illustrating the geological evolution of the study area, its relationship with its kinematic evolution of transform margins, and the importance of each stage to the petroleum system recognized in this work. See text for detailed explanation. Total organic carbon (*TOC*) content is measured in weight percent. The amount of hydrocarbons formed during thermal pyrolysis (S_2; milligrams of HC per gram of rock) is used to estimate the source-rock generation potential. The formula for hydrogen index (*HI*) is ($HI = [S_2/TOC] \times 100$ in mg HC/g *TOC*). Modified from Mascle and Blarez (1987) and Mercier de Lépinay et al. (2016). CFZ = Chain Fracture Zone; RFZ = Romanche Fracture Zone; SU = seismic unit.

canyons and reach the continental slope, causing an increase of sedimentary burden (a function of sedimentation rate) in unstable areas, such as along the continental slope, creating an ideal setting for the development of gravity tectonics. The absence of important gravity systems in the Mundaú subbasin may be attributed to the lower sedimentation rates recorded here, which are in turn related to the absence of important rivers such as the Amazonas and Parnaíba.

Nemčok et al. (2016) state that an important control on the structure is the need for faults to accommodate the spreading centers along the transform margin, ceasing their activity at different times depending on their location between the landward and oceanward ends of the transform faults. In the distal Mundaú subbasin some faults were active into the upper Oligocene, as suggested by the flower structures in Figures 7D and 8D soling out in horizon 5. In addition, other subvertical faults intersect the drift

sequence, some of them reaching horizon 6 (intra-Miocene) (Figures 8B, 9C). These faults indicate that strike-slip tectonics affected the Mundaú subbasin until the late Cenozoic and influenced the study area well after the beginning of the drift stage.

Transpressional structures such as shale ridges, en echelon folds and transpressive belts (e.g., Tutóia, Atlantic, and Ceará Highs) (Figure 1), as mapped by Zalán (1985) in the Piauí–Camocim and Acaraú subbasins, were not identified in the Mundaú subbasin. Typical structures of transform margins such as marginal ridges and marginal plateaus (Mercier de Lépinay et al., 2016) were also not found in the study area. The relative absence of transpressional structures can be attributed to the relative location of the Mundaú subbasin in relation to the transform faults. It is suggested that the Piauí–Camocim subbasin is closer to the outer corner of a transform fault, whereas the Mundaú subbasin is closer to its inner corner (Basile, 2015; Mercier de Lépinay et al., 2016) (Figure 11). Basile (2015) explained that inner corners are not affected by transform faults, but only by smaller, secondary transfer structures such as horse-tail splays connecting strike-slip and normal faults. In contrast, the outer corner is the part of the transform margin that experiences the longest transform fault activity. Mascle and Blarez (1987) considered these outer corner regions as favorable to the formation of marginal ridges and transform related tectonics (Figure 11). Thus, the Mundaú subbasin is less "typical" of a transform setting when compared to the Piauí–Camocim subbasin. The Mundaú subbasin is an oblique rift (Matos et al., 1996) developed closer to the inner corner of the Chain transform fault, constituting a divergent segment of the equatorial margin and evolving in a transtensional tectonic regime.

Comparing Petroleum Systems in the Proximal and Distal Domains of the Mundaú Subbasin

In the proximal domain of the Mundaú subbasin, four petroleum systems are found: Paracuru–Ubarana, Paracuru–Paracuru, Mundaú–Paracuru, and Mundaú–Mundaú (Costa et al., 1990). The Paracuru–Ubarana petroleum system consists of turbiditic sandstones (reservoir) interbedded with shales (seal) from the Ubarana Formation. The oil found in this stratigraphic play was generated in the Paracuru Formation and hydrocarbon migration occurred along normal faults. The Espada, Xaréu and Atum fields are examples of this petroleum system (Costa et al., 1990).

In the distal domain, gas was found in the Ubarana Formation (Table 3). The reservoirs are hyaline sandstones intercalated with greenish dark to light shales. Hydrocarbons accumulated in stratigraphic traps similar to those recorded in the proximal domain. The potential source rocks of the Ubarana Formation have excellent $TOC\%$ values, but they are immature (Figure 10C). The gas found in this formation migrated from transitional source rocks (Paracuru Formation with gas and condensate generation potential; Tables 1, 2). The migration occurred along the transtensional faults mapped around the Pecém well (Figures 5, 9).

The Paracuru–Paracuru petroleum system occurs in the shallow-water Mundaú subbasin in a mixed (structural–stratigraphic) play (Costa et al., 1990). This play is characterized by truncation of transitional sandstones of the Paracuru Formation, associated with the faults that tilted the blocks. The oil found in reservoir intervals was predominantly generated in shales that occur intercalated with the sandstones, but also reveals contributions of synrift source rocks (Costa et al., 1990).

This mixed play also occurs in the distal domain of the Mundaú subbasin (Pecém well). Here, Aptian early-mature source rocks within the oil window (Figures 5, 9–11; Tables 1, 2) were able to expel hydrocarbons. These hydrocarbons accumulated very close to where they were produced (Figure 10A). The upper Aptian reservoirs are located on the footwall of a normal fault truncated by an erosional surface (Figure 5H, J). The well tests undertaken in theses reservoirs were markedly successful (Table 3).

The possibility of hydrocarbon accumulations on the rollover anticline of the hanging-wall block is not ruled out (Figure 5D). The rollover anticline is formed by reversal of regional dip by rotation of the downthrown block along a normal fault. The rollover anticline is the area where a dome-shaped trap was formed. If the Uruburetama Member (SU4) also acts as an effective seal in this dome, hydrocarbons can accumulate at the anticlinal crest, as observed in the Gulf Coast, Niger Delta, Campos, Santos, and Kwanza Basins (Krézsek et al., 2007; Quirk et al., 2012). According to Jackson and Galloway

(1984) and Sheriff and Geldart (1995), this type of trap is significant to the hydrocarbon industry. Therefore, it is also important to consider rollover anticlines in the Mundaú subbasin as potential structural traps for hydrocarbons.

Mundaú–Mundaú and Mundaú–Paracuru petroleum systems were not found in the distal domain of the Mundaú subbasin. However, the interpretation of a thick sequence (SU1) with high-amplitude internal reflections (Figures 4C, 5I, 7E, 8D), the increasing TOC values with depth (Table 2), and the current knowledge about correlative source rocks on the conjugate African margin and other Brazilian basins, suggest that an important source interval may exist in the basal synrift strata of the Ceará Basin. In the neighboring Potiguar Basin, the most important source is the Berriasian Pendências Formation, composed of lacustrine and gravity-flow deposits (Pessoa Neto et al., 2007) (Figure 11). In the Campos Basin, the oil was chiefly generated by Aptian lacustrine shales of the Coqueiros Formation (Lagoa Feia Group) (Chang et al., 1992, Winter et al., 2007). Similarly, the Guaratiba Formation is responsible for oil generation in the Santos Basin. Here, oil was generated in rocks deposited in saline lacustrine environments during the Aptian (Chang et al., 2008). In addition, Abu et al. (2010) suggest the presence of a Cretaceous petroleum system in the Accra-Keta Basin with at least two key mature source rocks, with one being Lower Cretaceous lacustrine shale with types II and III kerogen. Thus, it is suggested that oil may be generated and accumulated in older sections of the Mundaú Formation not yet reached by the Pecém well.

CONCLUSIONS

Three tectono-stratigraphic sequences were recognized in deep-water Mundaú subbasin, and subdivided in seven SU. Major conclusions are as follows.

1. The SU1 and SU2 are lower Aptian sequences correlating with the Mundaú Formation. The SU3 is an upper Aptian transitional sequence correlating with the Paracuru Formation. This breakup sequence sensu Soares et al. (2012) marks a gradual transition spanning the onset of the lithospheric breakup event to the establishment of thermal relaxation as the main control on subsidence of the continental margin.

2. The SU4 is an Upper Cretaceous transgressive drift sequence corresponding to the Uruburetama Member of the Ubarana Formation. The SU5 and SU6 are Cenozoic regressive drift sequences which, together with the transgressive SU7, correspond with the Itapagé Member of the Ubarana Formation.

3. Different tectonic domains were interpreted in this work: proximal, distal, and RFZ domains. Flower structures and high-angle faults were mapped in the distal and RFZ domains. However, typical structures of transform margins, such as marginal ridges and marginal plateaus, were not mapped in the Mundaú subbasin. Instead, the study area was predominantly deformed by transtensional movements typical of an oblique rift. Hence, it is proposed that the study area evolved near to the inner corner of the Chain transform fault.

4. The synrift stage generated tilt blocks filled by the Mundaú Formation. During the transitional stage, diachronous synrift faults propagated vertically into the upper Aptian breakup sequence (Paracuru Formation). Shales with good to excellent source potential were deposited together with thin sandstone layers, respectively comprising source and reservoir intervals.

5. The drift stage begins with the Uruburetama Member shale deposition. These shales are competent seal intervals.

6. Despite the recognition in this work of the Mundaú Formation as a moderate to good source unit, the results showed that hydrocarbons in the Paracuru Formation are autochthonous and were accumulated very close to their source.

This work confirms that the Paracuru Formation comprises both the main source and reservoir intervals in the distal domain of the Mundaú subbasin, constituting a Paracuru–Paracuru petroleum system. It is suggested that the presence of this transitional system may continue in other deep-water basins of the BEM. Furthermore, the existence of the following cannot be ruled out: (1) source rocks and reservoirs in the synrift Mundaú Formation, which are related to the onset of rifting in equatorial Brazil, and (2) reservoir intervals in the thicker

parts of the Ubarana Formation, a unit associated with the migration of hydrocarbons from synrift and transitional source rocks into drift reservoirs.

REFERENCES CITED

Abu, C., M. Francis, G. Milne, and N. Herbst, 2010, Play fairway analysis and hydrocarbon potential of the Keta Basin, deep water Ghana (abs.): AAPG African Regional Annual Conference, Abuja, Nigeria, November 14–19, 2010, accessed October 28, 2013, http://www.searchanddiscovery.com/abstracts/pdf/2010/african_regional/abstracts/ndx_abu.pdf.

Alves, T. M., and T.A. Cunha, 2018, A phase of transient subsidence, sediment bypass and deposition of regressive–transgressive cycles during the breakup of Iberia and Newfoundland: Earth and Planetary Science Letters, v. 484, 168–183, doi:10.1016/j.epsl.2017.11.054.

Antunes, A. F., E. F. Jardim de Sá, R. G. S. Araújo, and F. F. Lima Neto, 2008, Caracterização tectonoestrutural do Campo de Xaréu (Sub-Bacia de Mundaú, Bacia do Ceará – NE do Brasil): Abordagem multiescala e pluriferramental: Revista Brasileira de Geociencias, v. 38, no. 1, p. 88–105, doi:10.25249/0375-7536.2008381S88105.

Arens, G., J. R. Delteil, P. Valery, B. Damotte, L. Montadert, and P. Patriat, 1971, The continental margin of the Ivory Coast and Ghana, in F. M. Delany, ed., The geology of the east Atlantic continental margin: Africa: Minneapolis, Minnesota, Institute of Geological Sciences, p. 61–78.

Basile, C., 2015, Transform continental margins — Part 1: Concepts and models: Tectonophysics, v. 661, p. 1–10, doi:10.1016/j.tecto.2015.08.034.

Basile, C., J. Mascle, M. Popoff, J. P. Bouillin, and G. Mascle, 1993, The Côte d'Ivoire-Ghana transform margin: A marginal ridge structure deduced from seismic data: Tectonophysics, v. 222, no. 1, p. 1–19, doi:10.1016/0040-1951(93)90186-N.

Beltrami, C. V., L. E. M. Alves, and F. J. Feijó, 1994, Bacia do Ceará: Boletim de Geociências da Petrobras, v. 8, no. 1, p. 117–125.

Ben-Avraham, Z., C. J. H. Hartnady, and K. A. Kitchin, 1997, Structure and tectonics of the Agulhas-Falkland fracture zone: Tectonophysics, v. 282, no. 1–4, p. 83–98, doi:10.1016/S0040-1951(97)00213-8.

Bird, D., 2001, Shear margins: Continent-ocean transform and fracture zone boundaries: The Leading Edge, v. 20, no. 2, p. 150–159, doi:10.1190/1.1438894.

Bischoff, J. L., and T. L. Henyey, 1974, Tectonic elements of the central part of the Gulf of California: Geological Society of America Bulletin, v. 85, no. 12, p. 1893–1904, doi:10.1130/0016-7606(1974)85<1893:TEOTCP>2.0.CO;2.

Bjørlykke, K., 2010, Petroleum geoscience: From sedimentary environments to rock physics: Berlin, Springer-Verlag, 508 p., doi:10.1007/978-3-642-02332-3.

Catuneanu, O., 2006, Principles of sequence stratigraphy, 1st ed.: Amsterdam, Elsevier Science, 386 p.

Chang, H. K., M. L. Assine, F. S. Corrêa, J. S. Tinen, A. C. Vidal, and L. Koike, 2008, Sistemas petrolíferos e modelos de acumulação de hidrocarbonetos na Bacia de Santos: Revista Brasileira de Geociencias, v. 38, no. 2, p. 29–46, doi:10.25249/0375-7536.2008382S2946.

Chang, H. K., R. O. Kowsmann, A. M. F. Figueiredo, and A. A. Bender, 1992, Tectonics and stratigraphy of the East Brazil Rift System: An overview: Tectonophysics, v. 213, no. 1–2, p. 97–138, doi:10.1016/0040-1951(92)90253-3.

Cobbold, P. R., K. Mourgues, and K. Boyd, 2004, Mechanism of thin-skinned detachment in the Amazon Fan: Assessing the importance of fluid overpressure and hydrocarbon generation: Marine and Petroleum Geology, v. 21, no. 8, p. 1013–1025, doi:10.1016/j.marpetgeo.2004.05.003.

Condé, V. C., C. C. Lana, O. C. Pessoa Neto, E. H. Roesner, J. M. Morais Neto, and D. C. Dutra, 2007, Bacia do Ceará: Boletim de Geociências da Petrobras, v. 15, no. 2, p. 347–355.

Costa, I. G., C. V. Beltrami, and L. E. M. Alves, 1990, A evolução tectono-sedimentar e o "habitat" do óleo da Bacia do Ceará: Rio de Janeiro, Petrobras/Depex, Anais, Seminário de Interpretação Exploratória 1, p. 75–85.

Dailly, P., T. Henderson, E. Hudgens, K. Kanschat, and P. Lowry, 2013, Exploration for Cretaceous stratigraphic traps in the Gulf of Guinea, West Africa and the discovery of the Jubilee Field: A play opening discovery in the Tano Basin, Offshore Ghana: Geological Society, London, Special Publications 2013, v. 369, p. 235–248, doi:10.1144/SP369.12.

Davison, I., T. Faull, J. Greenhalgh, E. O. Beirne, and I. Steel, 2016, Transpressional structures and hydrocarbon potential along the Romanche Fracture Zone: A review, in M. Nemčok, S. Rybár, S. T. Sinha, S. A. Hermeston, and L. Ledvényiová, eds., Transform margins: Development, controls and petroleum systems, Geological Society, London, Special Publications 2016, v. 431, p. 235–248, doi:10.1144/SP431.2.

de Caprona, G. C., 1992, The continental margin of western Côte D'Ivoire: Structural framework inherited from intra-continental shearing, Ph.D. thesis, Pierre and Marie Curie University, Paris, 150 p.

Delteil, J. -R., P. Valery, L. Montadert, C. Fondeur, P. Patriat, and J. Mascle, 1974, Continental margin in the northern part of the Gulf of Guinea, in C. A. Burk and C. L. Drake, eds., The geology of continental margins: New York, Springer-Verlag, p. 297–311, doi:10.1007/978-3-662-01141-6_22.

Dingle, R. V., 1973, Post-Palaeozoic stratigraphy of the eastern Agulhas bank, South African continental margin: Marine Geology, v. 15, no. 1, p. 1–23, doi:10.1016/0025-3227(73)90019-4.

Durand, B., 1988, Understanding of HC migration in sedimentary basins (present state of knowledge): Organic Geochemistry, v. 13, no. 1–3, p. 445–459, doi:10.1016/0146-6380(88)90066-6.

Eagles, G., 2007, New angles on South Atlantic opening: Geophysical Journal International, v. 168, no. 1, p. 353–361, doi:10.1111/j.1365-246X.2006.03206.x.

El Nady, M. M., F. S. Ramadan, M. M. Hammad, and N. M. Lotfy, 2015, Evaluation of organic matters, hydrocarbon potential and thermal maturity of source rocks based on geochemical and statistical methods: Case study of source rocks in Ras Gharib oilfield, central Gulf of Suez, Egypt: Egyptian Journal of Petroleum, v. 24, no. 2, p. 203–211, doi:10.1016/j.ejpe.2015.05.012.

Elvsborg, A., and J. Dalode, 1985, Benin hydrocarbon potential looks promising: Oil & Gas Journal, v. 82, p. 126–131.

Espitalié, J., G. Deroo, and F. Marquis, 1985, La pyrolise Rock-Eval et ses applications. Première partie: Revue de l'Institut Français du Pétrole, v. 40, no. 5, p. 563–579, doi:10.2516/ogst:1985035.

Espitalié, J., J. L. Laporte, M. Madec, F. Marquis, P. Leplat, J. Paulet, and A. Boutefeu, 1977, Methode rapide de caracterisation des roches meres, de leur potential petrolier et de leur degre d'evolution: Revue de l'Institut Français du Pétrole, v. 32, no. 1, p. 23–42, doi:10.2516/ogst:1977002.

Faugères, J. -C., D. A.V. Stow, P. Imbert, and A. R. Viana, 1999, Seismic features diagnostic of contourite drifts: Marine Geology, v. 162, no. 1, p. 1–38, doi:10.1016/S0025-3227(99)00068-7.

Genik, G. J., 1992, Regional framework and structural aspects of rift basins in Niger, Chad and the Central African Republic (C.A.R.), in P. A. Ziegler ed., Geodynamics of rifting, volume II case history studies on rifts: North and South America and Africa: Tectonophysics, v. 213, p. 169–185, doi:10.1016/0040-1951(92)90257-7.

Gorini, M. A., 1993, A margem equatorial brasileira: uma visão geotectônica: Resumos expandidos do Congresso Internacional da Sociedade Brasileira de Geofísica 3: Sociedade Brasileira de Geofísica, v. 2, p. 1355–1357.

Gorini, M. A., and G. M. Bryan, 1976, The tectonic fabric of the equatorial and adjoining continental margins; Gulf of Guinea to northeastern Brazil, Ph.D. thesis, Columbia University, New York, 382 p.

Guiraud, R., and J. C. Maurin, 1992, Early Cretaceous rifts of Western and Central Africa: An overview: Tectonophysics, v. 213, no. 1–2, p. 153–168, doi:10.1016/0040-1951(92)90256-6.

Hunt, J. M., 1996, Petroleum geochemistry and geology, 2nd ed.: New York, W. E. Freeman, 501 p.

Jackson, M. P. A., and W. E. Galloway, 1984, Growth faults and petroleum traps: Unit 12: Principles, in Structural and depositional styles of Gulf Coast tertiary continental margins: Application to hydrocarbon exploration: AAPG Continuing Education Course Notes 25, p. 55–59.

Jovane, L., J. J. P. Figueiredo, D. P. V. Alves, D. Iacopini, M. Giorgioni, P. Vannucchi, D. S. Moura, et al., 2016, Seismostratigraphy of the Ceará Plateau: Clues to decipher the Cenozoic evolution of Brazilian equatorial margin: Frontiers of Earth Science, v. 4, no. 90, p. 1–14, doi:10.3389/feart.2016.00090.

Keen, C., W. Kay, and W. R. Roest, 1990, Crustal anatomy of a transform continental margin: Tectonophysics, v. 173, no. 1–4, p. 527–529, 535–544, doi:10.1016/0040-1951(90)90244-3.

König, M., and W. Jokat, 2006, The Mesozoic breakup of the Weddell Sea: Journal of Geophysical Research: Solid Earth, v. 111 no. B12, p. B12102, doi:10.1029/2005JB004035.

Krézsek, C., J. Adam, and D. Grujic, 2007, Mechanics of fault and expulsion rollover systems developed on passive margins detached on salt: Insights from analogue modelling and optical strain monitoring, in S. J. Jolley, D. Barr, J. J. Walsh, and R. J. Knipe, eds., Structurally complex reservoirs, Geological Society, London, Special Publications 2007, v. 292, p. 103–121, doi:10.1144/SP292.6.

Krueger, A., M. Murphy, K. Burke, and E. Gilbert, 2014, The Brazilian equatorial margin: A snapshot in time of an oblique rifted margin: Search and Discovery article 30325, accessed July 15, 2017, http://www.searchanddiscovery.com/documents/2014/30325krueger/ndx_krueger.pdf .

Lonsdale, P., 1985, A transform continental margin rich in hydrocarbons, Gulf of California: AAPG Bulletin, v. 69, no. 7, p. 1160–1180.

Lorenzo, J. M., J. C. Mutter, and R. L. Larson, 1991, Development of the continent-ocean transform boundary of the southern Exmouth Plateau: Geology, v. 19, no. 8, p. 843–846, doi:10.1130/0091-7613(1991)019<0843:DOTCOT>2.3.CO;2.

Lorenzo, J. M., and P. Wessel, 1997, Flexure across a continent–ocean fracture zone: The northern Falkland/Malvinas Plateau, South Atlantic: Geo-Marine Letters, v. 17, no. 1, p. 110–118, doi:10.1007/s003670050015.

Macdonald, D., I. Gomez-Perez, J. Franzese, L. Spalleti, L. Lawver, L. Gahagan, I. Dalziel, et al., 2003, Mesozoic break-up of SW Gondwana: Implications for regional hydrocarbon potential of the southern South Atlantic: Marine and Petroleum Geology, v. 20, no. 3–4, p. 287–308, doi:10.1016/S0264-8172(03)00045-X.

Mascle, J., and E. Blarez, 1987, Evidence for transform margin evolution from the Ivory Coast–Ghana continental margin: Nature, v. 326, no. 6111, p. 378–381, doi:10.1038/326378a0.

Mascle, J., E. Blarez, and M. Marinho, 1988, The shallow structures of the Guinea and Ivory Coast-Ghana transform margins: Their bearing on the Equatorial Atlantic Mesozoic evolution: Tectonophysics, v. 155, no. 1–4, p. 193–209, doi:10.1016/0040-1951(88)90266-1.

Matos, R. M. D., 1992, The northeast Brazilian rift system: Tectonics, v. 11, no. 4, p. 766–791, doi:10.1029/91TC03092.

Matos, R. M. D., 1999, History of the northeast Brazilian rift system: Kinematic implications for the break-up between Brazil and West Africa, in N. R. Cameron, R. H. Bate, and V. S. Clure, eds., The oil and gas habitats of the South Atlantic: Geological Society, London, Special Publications 1999, v. 153, p. 55–73, doi:10.1144/GSL.SP.1999.153.01.04.

Matos, R. M. D., R. N. Waick, and V. P. C. Pimentel, 1996, Bacia do Ceará (Mundaú): Uma fase rifte convencional!?, *in* Sociedade Brasileira de Geologia/Núcleo Bahia-Sergipe, Anais do 39° Congresso Brasileiro de Geologia, v. 5, p. 358–362.

Mercier de Lépinay, M., L. Loncke, C. Basile, W. R. Roest, M. Patriat, A. Maillard, and P. De Clarens, 2016, Transform continental margins – Part 2: A worldwide review: Tectonophysics, v. 693, p. 96–115, doi:10.1016/j.tecto.2016.05.038.

Mitchum, R. M. Jr., P. R. Vail, and J. B. Sangree, 1977, Seismic stratigraphy and global changes of sea level, Part 6: Stratigraphy interpretation of seismic reflection patterns in deposition sequences, *in* C. E. Payton, ed., Seismic stratigraphy–Applications to hydrocarbons exploration: AAPG Memoir 26, p. 117–133, doi:10.1306/M26490C8.

Mizusaki, A. M. P., A. Thomaz Filho, E. J. Milani, and P. Césero, 2002, Mesozoic and Cenozoic igneous activity and its tectonic control in northeastern Brazil: Journal of South America Earth Sciences, v. 15, p. 183–198, doi:10.1016/S0895-9811(02)00014-7.

Moore, D. G., and J. R. Curray, 1982, Geologic and tectonic history of the Gulf of California: Deep Sea Drilling Project Initial Reports, v. 64, p. 1279–1294, doi:10.2973/dsdp.proc.64.169.1982.

Morais Neto, J. M., O. C. Pessoa Neto, C. C. Lana, and P. V. Zalán, 2003, Bacias sedimentares brasileiras: Bacia do Ceará: Phoenix, v. 57, p. 1–6.

Moulin, M., D. Aslanian, and P. Unternehr, 2010, A new starting point for the south and equatorial Atlantic Ocean: Earth-Science Reviews, v. 98, no. 1–2, p. 1–37, doi:10.1016/j.earscirev.2009.08.001.

Nemčok, M., A. Henk, R. Allen, P. J. Sikora, and C. Stuart, 2012, Continental break-up along strike-slip fault zones; Observations from the equatorial Atlantic, *in* W. U. Mohriak, A. Danforth, P. J. Post, D. E. Brown, G. C. Tari, M. Nemčok, and S. T. Sinha, eds., Conjugate divergent margins: Geological Society, London, Special Publications 2012, v. 369, p. 537–556. doi:10.1144/SP369.8.

Nemčok, M., A. Henk, and M. Molčan, 2015, The role of pre-break-up heat flow on thermal history of transform margin, *in* M. Nemčok, S. Rybár, S. T. Sinha, S. A. Hermeston, and L. Ledvényiová, eds., Transform margins: Development, controls and petroleum systems, Geological Society, London, Special Publications 2015, v. 431, p. 249–271, doi:10.1144/SP431.4.

Nemčok, M., S. Rybár, S. T. Sinha, S. A. Hermeston, and L. Ledvényiová, 2016, Transform margins: Development, controls and petroleum systems – An introduction, *in* M. Nemčok, S. Rybár, S. T. Sinha, S. A. Hermeston, and L. Ledvényiová, eds., Transform margins: Development, controls and petroleum systems, Geological Society, London, Special Publications 2016, v. 431, p. 1–38., doi:10.1144/SP431.15.

Nürnberg, D., and R. D. Müller, 1991, The tectonic evolution of the South Atlantic from Late Jurassic to present: Tectonophysics, v. 191, no. 1–2, p. 27–53, doi:10.1016/0040-1951(91)90231-G.

Oliveira, M. J. R., P. V. Zalán, J. L. Caldeira, A. Tanaka, P. Santarem, I. Trosdtorf Jr., and A. Moraes, 2012, Linked extensional-compressional tectonics in gravitational systems in the equatorial margin of Brazil, *in* O. Gao, ed., Tectonics and sedimentation: Implications for petroleum systems: AAPG Memoir 100, p. 159–178, doi:10.1306/13351552M1003532.

Pankhurst, R. J., R. A. J. Trouw, B. B. Brito Neves, and M. J. De Wit, 2008, West Gondwana: Pre-Cenozoic correlations across the South Atlantic region, Geological Society, London, Special Publications 2008, v. 294, 404 p.

Pessoa Neto, O. C., U. M. Soares, J. G. F. Silva, E. H. Roesner, C. P. Florencio, and C. A. V. Souza, 2007, Bacia Potiguar: Boletim de Geociências da Petrobras, v. 15, no. 2, p. 357–369.

Peters, K. E., 1986, Guidelines for evaluating petroleum source using programmed pyrolysis: AAPG Bulletin, v. 70, no. 3, p. 318–329.

Peters, K. E., and M. R. Cassa, 1994, Applied source rock geochemistry, *in* L. B. Magoon and W. G. Dow, eds., The petroleum system – From source to trap: AAPG Memoir 60, p. 93–117.

Quirk, D. G., N. Schødt, B. Lassen, S. J. Ings, D. Hsu, K. K. Hirsch, and C. V. Nicolai, 2012, Salt tectonics on passive margins: Examples from Santos, Campos and Kwanza basins: Geological Society, London, Special Publications 2012, v. 363, p. 207–244, doi:10.1144/SP363.10.

Rabbani, A. R., and M. R. Kamali, 2005, Source rock evaluation and petroleum geochemistry, offshore SW Iran: Journal of Petroleum Geology, v. 28, no. 4, p. 413–428, doi:10.1111/j.1747-5457.2005.tb00091.x.

Reid, I. D., and H. R. Jackson, 1997, A review of three transform margins off eastern Canada: Geo-Marine Letters, v. 17, no. 1, p. 87–93, doi:10.1007/s003670050012.

Reis, A. T., E. Araújo, C. G. Silva, A. M. Cruz, C. Gorini, L. Droz, S. Migeon, R. Perovano, I. King, and F. Bache, 2016, Effects of a regional décollement level for gravity tectonics on late Neogene to recent large-scale slope instabilities in the Foz do Amazonas Basin, Brazil: Marine and Petroleum Geology, v. 75, p. 29–52, doi:10.1016/j.marpetgeo.2016.04.011.

Reis, A. T., R. Perovano, C. G. Silva, B. C. Vendeville, E. Araujo, C. Gorini, and V. Oliveira, 2010, Two-scale gravitational collapse in the Amazon Fan: A coupled system of gravity tectonics and mass-transport processes: Journal of the Geological Society, v. 167, no. 3, p. 593–604, doi:10.1144/0016-76492009-035.

Rowan, M. G., M. P. A. Jackson, and B. D. Trudgil, 1999, Salt-related fault families and fault welds in the northern Gulf of Mexico: AAPG Bulletin, v. 83, no. 9, p. 1454–1484.

Scrutton, R. A., 1973, Structure and evolution of the sea floor south of South Africa: Earth and Planetary Science Letters, v. 19, no. 2, p. 250–256, doi:10.1016/0012-821X(73)90125-8.

Scrutton, R. A., 1976, Crustal structure at the continental margin south of South Africa: Geophysical Journal of the Royal Astronomical Society, v. 44, no. 3, p. 601–623, doi:10.1111/j.1365-246X.1976.tb00296.x.

Scrutton, R. A., 1979, On sheared passive continental margins: Tectonophysics, v. 59, no. 1–4, p. 293–305, doi:10.1016/0040-1951(79)90051-9.

Scrutton, R. A., 1982, Crustal structure of sheared passive continental margins, in Dynamics of Passive Margins: Washington, DC, American Geophysical Union Geodynamics Series 6, p. 133–139.

Sheriff, R. E., and L. P. Geldart, 1995, Exploration seismology, 2nd ed.: Cambridge, United Kingdom, Cambridge University Press, 351 p., doi:10.1017/CBO9781139168359

Silva, C. G., E. F. S. Araújo, A. T. Reis, R. Perovano, C. Gorini, B. C. Vendeville, and N. C. Albuquerque, 2010, Megaslides in the Foz do Amazonas Basin, Brazilian equatorial margin, in D. C. Mosher, R. C. Shipp, L. Moscardelli, J. D. Chaytor, C. D. P. Baxter, H. J. Lee, and R. Urgeles, eds., Submarine mass movements and their consequences. Advances in natural and technological hazards research: Dordrecht, the Netherlands, Springer-Verlag, v. 28, p. 581–591, doi:10.1007/978-90-481-3071-9_47

Silva, S. R. P., R. R. Maciel, and M. C. G. Severino, 1998, Cenozoic tectonics of Amazon Mouth Basin: Geo-Marine Letters, v. 18, no. 3, p. 256–262, doi:10.1007/s003670050077.

Smith, J. T., 1994, Petroleum system logic as an exploration tool in a frontier setting, in L. B. Magoon and W. G. Dow, eds., The petroleum system–From source to trap: AAPG Memoir 60, p. 25–49, doi:10.1306/M60585C2.

Soares, D. M., T. M. Alves, and P. Terrinha, 2012, The breakup sequence and associated lithospheric breakup surface: Their significance in the context of rifted continental margins (West Iberia and Newfoundland margins, North Atlantic): Earth and Planetary Science Letters, v. 355–356, p. 311–326, doi:10.1016/j.epsl.2012.08.036.

Szatmari, P., 2000, Habitat of petroleum along the South Atlantic margins, in M. R. Mello and B. J. Katz, eds., Petroleum systems of South Atlantic margins, AAPG Memoir 73, p. 69–75, doi:10.1306/M73705C6.

Todd, B. J., I. Reid, and C. E. Keen, 1988, Crustal structure across the Southwest Newfoundland transform margin: Canadian Journal of Earth Sciences, v. 25, no. 5, p. 744–759, doi:10.1139/e88-070.

van Krevelen, D. W., 1961, Coal: Typology, chemistry, physics, constitution: Amsterdam, Elsevier Science, 514 p.

Winter, W. R., R. J. Jahnert, and A. B. França, 2007, Bacia de Campos: Boletim de Geociências da Petrobras, v. 15, no. 2, p. 511–529.

Zalán, P. V., 1985, Tectonics and sedimentation of the Piauí-Camocim Sub-basin, Ceará Basin, offshore northeastern Brazil: Série Ciência-Técnica-Petróleo, no. 17, 71 p.

Zalán, P. V., E. P. Nelson, J. Warme, and T. L. Davis, 1985, The Piaui Basin: Rifting and wrenching in an equatorial Atlantic transform basin, in K. T. Biddle and N. Christie-Blick, eds., Strike-slip deformation, basin formation, and sedimentation: Tulsa, Oklahoma, SEPM Special Publication 37, p. 177–192, doi:10.2110/pec.85.37.0159.